REVIEW ARTICLE

Check for updates

Emerging heterogeneous catalysts for biomass conversion: studies of the reaction mechanism

Longfei Lin, [ab] Xue Han, [b] Buxing Han [*a] and Sihai Yang [*b]

The development of efficient catalysts to break down and convert woody biomass will be a paradigm shift in delivering the global target of sustainable economy and environment *via* the use of cheap, highly abundant, and renewable carbon resources. However, such development is extremely challenging due to the complexity of lignocellulose, and today most biomass is treated simply as waste. The solution lies in the design of multifunctional catalysts that can place effective control on substrate activation and product selectivity. This is, however, severely hindered by the lack of fundamental understanding of (i) the precise role of active sites, and (ii) the catalyst–substrate chemistry that underpins the catalytic activity. Moreover, active sites alone often cannot deliver the desired selectivity of products, and full understanding of the microenvironment of the active sites is urgently needed. Here, we review key recent advances in the study of reaction mechanisms of biomass conversion over emerging heterogeneous catalysts. These insights will inform the design of future catalytic systems showing improved activity and selectivity.

1. Introduction

The increasing concerns on the longevity of fossil fuels and current emissions of an astronomical amount of greenhouse gases are powerful drivers to develop new sustainable and environmentally-friendly chemical processes to produce fuels and feedstocks.[1,2] Biomass, which is produced from carbon dioxide (CO_2) and water through photosynthesis by plants or microbes, is a renewable resource of carbon. Lignocellulose is the most abundant biomass resource with an annual production of *ca.* >170 billion metric tonnes, but currently only <5% of the produced lignocellulose is utilised for conversion into value-added products and fuels while the majority is treated as

a Beijing National Laboratory for Molecular Sciences, Key Laboratory of Colloid and Interface and Thermodynamics, Institute of Chemistry, Chinese Academy of Sciences, Beijing, 100190, China. E-mail: hanbx@iccas.ac.cn

b Department of Chemistry, University of Manchester, Manchester, M13 9PL, UK. E-mail: Sihai.Yang@manchester.ac.uk

Dr Longfei Lin received his PhD in Chemistry (2017) from Université Pierre et Marie Curie under the supervision of Professor Hélène Lauron-Pernot. He worked as a postdoctoral researcher at the Department of Chemistry, University of Manchester (2017–2020). In 2021, Dr Lin joined the Institute of Chemistry, Chinese Academy of Sciences, as an academic member of staff. His research interest lies in biomass conversion over new solid cata-

Longfei Lin

lysts, particularly in understanding the essential relationship between the reaction performance and active sites/structure of the catalysts by combined experimental and computational techniques.

Dr Xue Han received her BSc from Peking University in 2007 and PhD in Chemistry from the University of Nottingham in 2010 under the supervision of Sir Professor Martyn Poliakoff. She is currently a Research Fellow at the Department of Chemistry, University of Manchester. Her research interest lies in the development of functional porous materials for the capture and conversion of gaseous air pollutants, such as

Xue Han

NH_3, NO_x and SO_2, as well as separation and catalysis of valuable organic compounds. The research will promote the development of a clean-air future.

11270 | *Chem. Soc. Rev.*, 2021, 50, 11270–11292

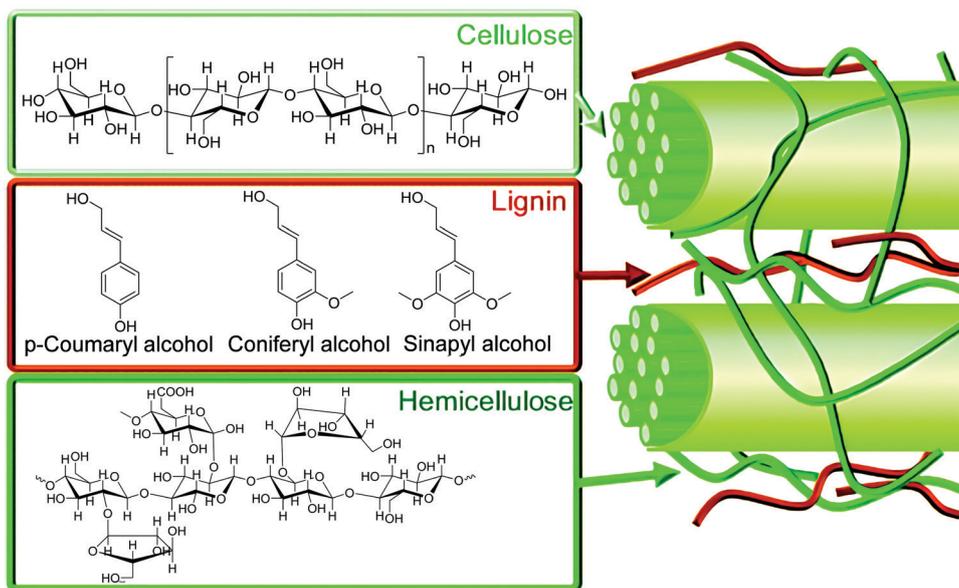This journal is © The Royal Society of Chemistry 2021

Fig. 1 Structures of cellulose, hemicellulose, and lignin components of lignocellulosic biomass and associated molecular building blocks. Reproduced with permission from ref. 4, Copyright 2012 Royal Society of Chemistry.

waste owing to the lack of efficient catalysts to break down and convert lignocellulose.[3]

Lignocellulosic biomass mainly contains cellulose, hemicellulose and lignin (Fig. 1).[4] Cellulose is a homopolymer consisting of β-D-glucopyranose units linked by β-glycosidic bonds, and accounts for 40–50% of lignocellulosic biomass. Hemicellulose is a branched polymer with low degrees of polymerisation (ca. 200). Hemicellulose is composed of pentose, hexose and uronic acids, and accounts for 15–30% of lignocellulose. Lignin, rich in aromatic functionalities, is a heavily cross-linked, complex polymer with coumaryl, coniferyl and sinapyl alcohols, accounting for 15–30% of lignocellulosic biomass.[4] Due to the complex and highly robust structure of

lignocellulosic biomass, energy-efficient and cost-effective production of chemicals and fuels from lignocellulosic biomass remains an extremely challenging target for both academia and industry.

One state-of-the-art strategy relies on the thermochemical treatment of lignocellulose to produce bio-oils or syngas by pyrolysis or gasification, respectively, coupled with subsequent catalytic upgrading to produce hydrocarbons.[5,6] These processes require high reaction temperature, and are generally non-selective and highly energy-intensive. Research efforts have been focused on developing new active catalysts to directly convert lignocellulose to liquid alkanes as transportation fuels

Professor Buxing Han received his PhD (1988) from the Institute of Chemistry, Chinese Academy of Sciences (CAS), and did postdoctoral research (1989–1991) at the University of Saskatchewan. He has been a Professor at the Institute of Chemistry, CAS, since 1993 and is the Chairman of Green Chemistry Committee, Chinese Chemical Society. He works on green chemistry and sustainable chemistry, especially the catalytic transformation of biomass and CO₂ into valuable chemicals. He is an Academician of Chinese Academy of Sciences, a Fellow of the Academy of Sciences for the Developing World (TWAS), and a Fellow of the Royal Society of Chemistry.

Buxing Han

Dr Sihai Yang received his BSc and PhD in Chemistry from Peking University (2007) and the University of Nottingham (2010), respectively. He is currently a Reader in Inorganic Chemistry at the University of Manchester. Yang's group develops porous materials based upon stable metal–organic frameworks and zeolites for applications in clean-air technology, heterogeneous catalysis, separation and conductivity. He has made pioneering contributions for the application of cutting-edge techniques, such as synchrotron X-ray diffraction, spectroscopy, neutron diffraction and inelastic/quasi-elastic neutron scattering, to in situ and operando studies of many dynamic and complex chemical processes.

Sihai Yang

This journal is © The Royal Society of Chemistry 2021

Chem. Soc. Rev., 2021, **50**, 11270–11292 | **11271**

under mild conditions.[7] However, due to the complex composition of lignocellulose, it is almost impossible to obtain a single component product from a given one-pot process.[8] One promising solution is to pre-treat lignocellulose by supercritical CO_2,[9] ionic-liquid-assisted deconstruction,[10,11] or utilisation of deep eutectic solvents[12] to isolate cellulose, hemicellulose and lignin. According to their different properties, designed processes can then be applied to promote the selective conversion of each component into target chemicals and fuels for direct use.

An enormous amount of efforts have been devoted to converting biomass and derived materials *via* (hydro)pyrolysis, solvolysis, hydrogenolysis, hydrodeoxygenation (HDO), dehydration, oxidation and reduction of lignin, and "lignin-first" approach-based depolymerisation. Various homogeneous and heterogeneous catalysts have been employed, such as polyoxometalates, ionic liquids, zeolites, mesoporous silica, transition metal complexes, carbon materials, and supported metal particles.[3,10,13–18] Heterogeneous catalysts attract greater attention due to their advantages in separation, catalyst recycling and environmental impact.[19] However, there are difficulties and challenges with these processes due to limited catalyst stability, low yields of the product and poor selectivity, and thus the formation of complex mixtures of products. Downstream separation is costly and often even impossible;[20] indeed, the separation of chemical mixtures is often the bottleneck of modern chemical industries.[21] As a result, products derived from biomass are subject to high cost, thus restricting their widespread application and implementation within renewable energy cycles and supplies. Therefore, powerful drivers exist to design highly selective and robust production processes of liquid fuels and value-added chemicals for direct

use from biomass and its derivatives. Such design requires unambiguous understanding of the catalytic mechanism of active sites and their microenvironment within the emerging heterogeneous catalysts. Although several excellent reviews are published on the upgrading of biomass to fuels and chemicals from various aspects,[1,3,4,15,16,22–28] a review focused on the analysis of the catalytic mechanism for biomass conversion is not yet available in the literature to date.

The isotope-labelling technique,[29] nuclear magnetic resonance (NMR) spectroscopy,[30] synchrotron X-ray powder diffraction (SXPD),[31] X-ray absorption spectroscopy (XAS),[32] density functional theory (DFT) calculations and,[33] more recently, inelastic neutron scattering (INS)[7,34–36] have been employed to investigate the reaction mechanism of biomass conversion. INS has several advantages compared with the optical spectroscopies, such as infrared and Raman spectroscopy.[37–43] For example, INS is not subject to any optical selection rule, and all vibrations (0–4000 cm^{-1}) are allowed and, in principle, measurable in INS. INS spectra can be readily and accurately modelled by DFT: the intensities are proportional to the concentration of elements in the sample and the features in the spectra can be fully assigned. Last but not least, neutrons penetrate deeply into materials and pass readily through the walls of metal containers, making cell design straightforward. Thus, neutrons are ideally positioned to measure the bulk properties of materials, which is particularly beneficial to the study of species residing on the inner surface of porous catalysts.

This review assesses the reaction mechanism studied by the isotope-labelling technique, NMR, SXPD, XAS, INS and DFT, and particularly focuses on the binding interactions between substrates and catalysts during the conversion of biomass (Fig. 2). The reaction mechanism is closely related to (i) the
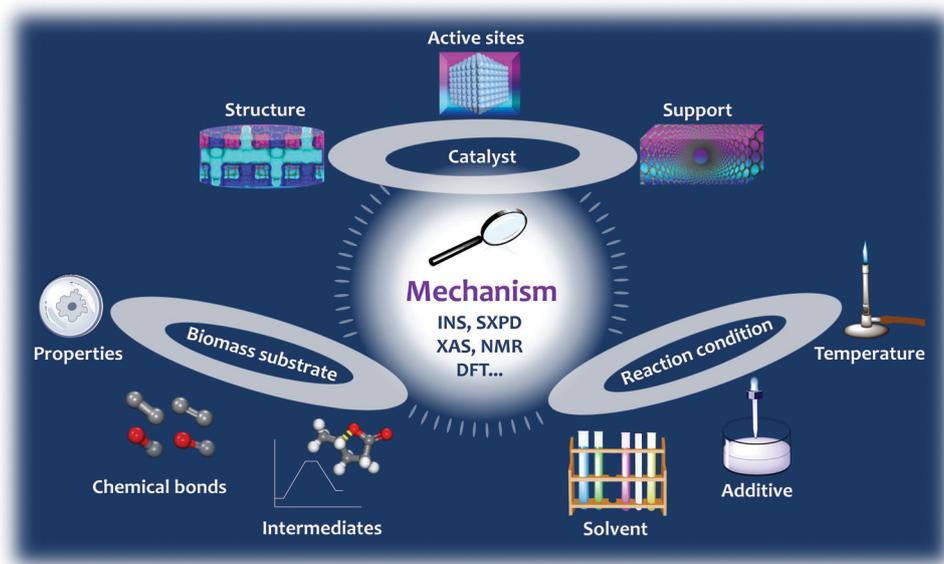

Fig. 2 Central theme of this review: analysis of the reaction mechanism of biomass conversion over emerging heterogeneous catalysts studied by the INS, SXPD, XAS, NMR, and DFT techniques. The structure, active site and support of the catalyst, properties, chemical bonds, intermediates of the substrate, and reaction conditions such as the solvent, additives and temperature are systematically reviewed.

11272 | *Chem. Soc. Rev.*, 2021, **50**, 11270–11292

This journal is © The Royal Society of Chemistry 2021

structure, active sites and support of the catalysts; (ii) the properties, nature of the chemical bonds, and intermediates of the substrates; and (iii) the reaction conditions, such as the solvent, pressure, additives and temperature, all of which will be discussed in detail (Fig. 2). The selected reactions in this review include hydrolysis, dehydration, isomerisation, aldol condensation, retro-aldol condensation, hydrogenation, hydrogenolysis, HDO, hydride shift, ring-opening, decarboxylation, Diels–Alder cycloaddition and oxidation (Scheme 1). The main body of this review is divided into four sections (Section 2–5) based on the end products of conversion of biomass. In Section 2, we discuss the reaction mechanism over porous solid catalysts for the production of aromatics and light olefins from biomass, because light olefins (ethylene, propylene and butene) and aromatics (benzene, toluene and xylene) are two families of the most important bulk chemicals with an annual global production of *ca.* 400 million[44] and 160 million tonnes,[45–47] respectively. They are basic building blocks for petrochemicals and polymers such as fibres, rubbers and plastics. In Section 3, we discuss the reaction mechanism for the synthesis of bio-plastics, for example the conversion of biomass to bio-plastic precursors, such as lactic acid and 2,5-furandicarboxylic acid (FDCA). In Section 4, we review the mechanism for the synthesis of liquid alkanes as fuels, which includes three strategies, (i) conversion of carbohydrate to 2,5-dimethylfuran (DMF), (ii) direct conversion of lignocellulose to liquid alkanes, and (iii) tandem production of long chain alkanes. Finally in Section 5, we summarise reactions involving C–O and
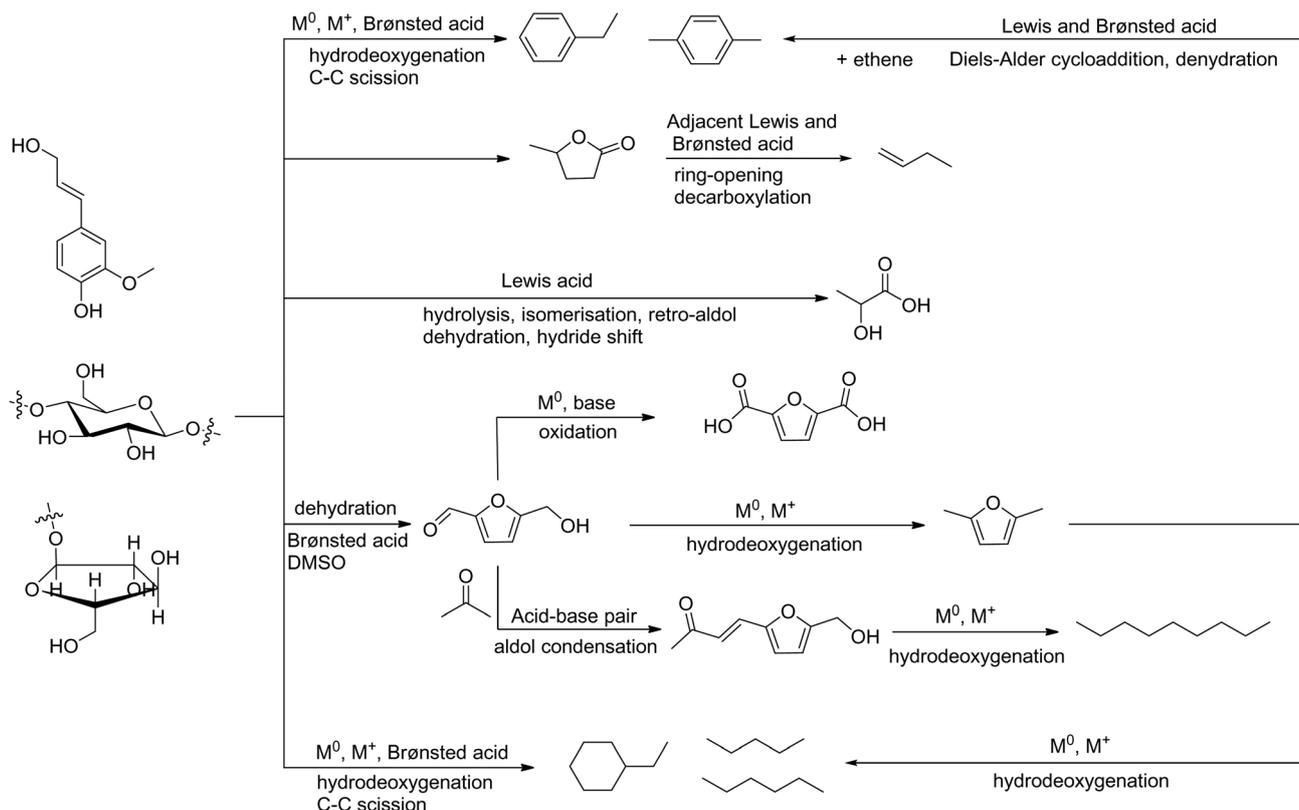
C–C bonds in biomass conversion. Instead of summarising the catalytic performance of various catalysts, this review attempts to analyse the nature of the active sites and mechanism of the reaction over selected heterogeneous catalysts to provide key insights into the design of future efficient systems for biomass conversion.

2. Reaction mechanism for the production of bulk chemicals

2.1. Production of aromatic compounds

Lignin is constructed from monomers of coumaryl, coniferyl and sinapyl alcohols, and represents the most abundant renewable source of aromatic compounds on the earth.[8,48] Because of its highly irregular polymeric structure and recalcitrant nature, efficient production of arenes from lignin is extremely challenging and often requires energy-intensive processes. For example, hydropyrolysis of lignin to aromatic compounds over the zeolite catalyst H-USY (yield: $\sim$30 wt%)[49] or Pd/HZSM-5 (yield: $\sim$44 wt%)[50] must operate at temperatures as high as 923 K.

Recently, an HDO reaction based on a porous Ru/Nb$_2$O$_5$ catalyst has been developed to convert lignin under milder conditions (523 K) to enable the almost quantitative cleavage of C$_{aromatic}$–O bonds and the complete removal of oxygen content from lignin, resulting in a total mass yield of 35.5 wt% and an exceptional arene selectivity of 71 wt%.[34] The HDO process over

Scheme 1 Routes of the catalytic conversion of lignocellulose to the representative chemicals and liquid fuels.

This journal is © The Royal Society of Chemistry 2021

Chem. Soc. Rev., 2021, **50**, 11270–11292 | 11273

Ru/Nb_2O_5 involves the cleavage of $C_{aromatic}$–O bonds but preserving the aromatic rings, which is difficult because the C–O bond in aryl ethers is strong, and the hydrogenation of aromatic rings is thermodynamically favoured. To reveal the catalytic mechanism behind the selective cleavage of $C_{aromatic}$–O bonds over Ru/Nb_2O_5, *operando* INS and DFT calculations were carried out. Phenol was selected as a model compound and several common catalyst supports such as ZrO_2, Al_2O_3, and TiO_2 were also studied for comparison to reveal the uniqueness of the Nb_2O_5 support. The INS study of adsorbed phenol on Nb_2O_5 showed that the intensity of the $C_{aromatic}$–OH bending mode reduced significantly, indicating that the $C_{aromatic}$–OH group of phenol interacts with Nb(v) sites and is deprotonated to form phenoxide bound to the vacant surface Nb(v) sites in an end-on model, resulting in the selective activation of C–O bonds. DFT calculations show distinct disassociation energies for the C–O bond of adsorbed phenoxide species on different catalysts. The energy required to cleave the C–O bonds in pristine phenol is 556 kJ mol^{-1}, which is reduced to 425, 500, 491 and 510 kJ mol^{-1} upon adsorption on Nb_2O_5, ZrO_2, Al_2O_3 and TiO_2, respectively (Fig. 3a and b). The largest reduction of energy (Δ = 131 kJ mol^{-1}) over Nb_2O_5 promotes the selective cleavage of C–O bonds, while it hinders the hydrogenation of the benzene ring owing to the confined adsorption geometry of phenoxide (end-on), leading to the observed high selectivity of arenes.
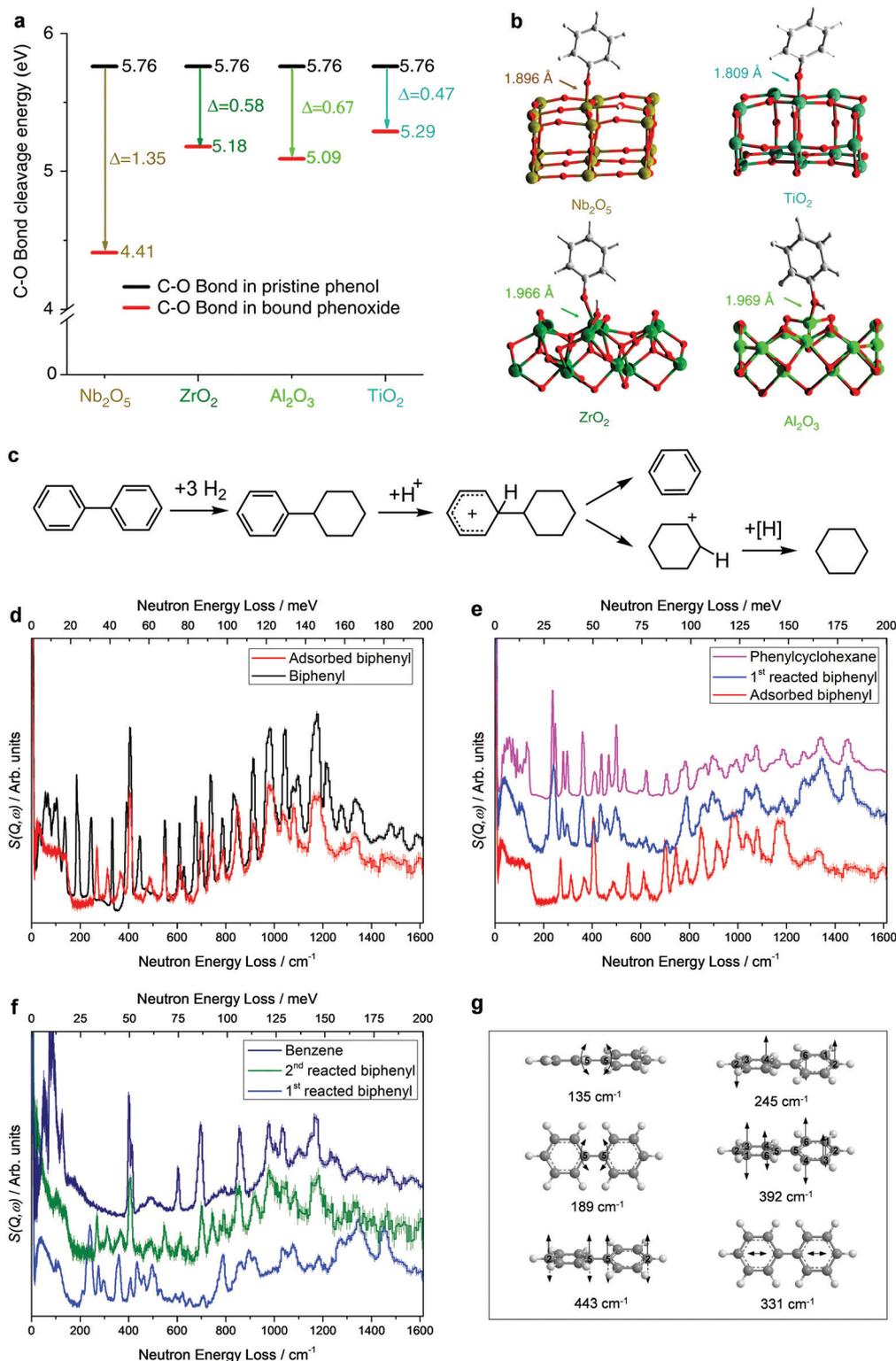
Compared with the cleavage of C–O bonds, the selective cleavage of interunit C–C bonds in lignin while preserving the aromatic ring is even more challenging, as the C–C bonds have notably higher dissociation energy (226–494 kJ mol^{-1}) than that of C–O bonds (209–348 kJ mol^{-1}). This naturally restricts the yield of aromatic monomers from the depolymerisation of lignin. A mesoporous multifunctional catalyst, Ru/$NbOPO_4$, combining NbO_x species and phosphates that contain strong Brønsted acid sites, has successfully broken down both interunit C–O and C–C bonds in lignin under mild conditions (583 K for 40 h).[35] To investigate the catalytic mechanism, biphenyl, which contains the C_5–C_5 linkage (dissociation energy of 481 kJ mol^{-1}), was selected as the model compound to study the cleavage of C–C bonds over Ru/$NbOPO_4$ by *operando* INS/DFT. It revealed four steps involved in the catalytic process (Fig. 3c–g). (i) The biphenyl molecule adsorbs onto the catalyst with a flat orientation. This results in the disappearance of the modes of out-of-plane and in-plane bending (135 and 189 cm^{-1}, respectively) of the C_5–C_5 bond. Meanwhile, the intensities of the deformational modes of the benzene rings at 628, 736, and 986 cm^{-1} reduced dramatically, indicating that both benzene rings of biphenyl adsorb on the catalyst (Fig. 3d). (ii) The adsorbed biphenyl molecule is partially protonated by the acid sites residing on the catalyst surface and an intermediate carbocation is formed. This is reflected by the shifts of the INS features at 245 and 392 cm^{-1}, corresponding to the twisting mode of the C–C bond within the benzene rings, to 269 and 366 cm^{-1}, respectively, and the shift of the peak at 331 cm^{-1} (assigned to the intra-ring stretching mode of benzene) to lower energy at 313 cm^{-1} (Δ = 18 cm^{-1}) (Fig. 3d). (iii) One benzene ring

of biphenyl is hydrogenated rapidly in the presence of H_2 to give phenylcyclohexane adsorbed on the catalyst solely *via* its phenyl group. This is observed directly by INS as upon the reaction in H_2 the peaks at 736 and 986 cm^{-1} (ring deformational modes of the phenyl group) have disappeared, and the peaks at 269, 313 and 366 cm^{-1} related to the intermediate carbocation shift to 275, 295 and 358 cm^{-1}, respectively, and several new features appeared which are all consistent with the INS spectrum of phenylcyclohexane (Fig. 3e). (iv) C_5–C_5 bonds are efficiently cleaved over Ru/$NbOPO_4$. In this step, the INS peaks for phenylcyclohexane significantly reduced or completely disappeared and features related to benzene (609, 405, 702, 857, 980, and 1185 cm^{-1}) appeared and increased in intensity as the reaction proceeds, demonstrating the cleavage of C_5–C_5 bonds of adsorbed phenylcyclohexane on Ru/$NbOPO_4$ (Fig. 3f). Besides the NbO_x species for the cleavage of C–O bonds, Ru/$NbOPO_4$ integrates Brønsted acid sites and Ru centres with moderate hydrogenation ability, which enables the cleavage of robust interunit C–C bonds to maximise the production of lignin monocyclic hydrocarbons.

In addition to lignin, aromatics can also be produced from derivatives of cellulose and hemicellulose.[51–56] Bio-derived furans can be converted into aromatics by a Diels–Alder (DA) cycloaddition with ethene or propene on Lewis acid sites, followed by dehydration on Brønsted acid sites.[51,52] Side reactions, such as the hydrolysis of DMF to 2,5-hexanedione and ethene oligomerisation, can occur on acid sites as well (Scheme 2).[52] DFT calculations demonstrate that the hydrolysis of DMF occurs more readily over beta zeolite with strong acid sites than over *t*-ZrO_2 with weak acid sites with an activation energy of 166 and 275 kJ mol^{-1}, respectively (Scheme 2). Ethene oligomerisation was also strongly favoured over the beta zeolite (Scheme 2).[52] Thus, the highly selective and efficient production of aromatics from furans requires weak acid sites and cooperation between Lewis and Brønsted acid sites. Moreover, the structure of the catalyst is one of the key factors for the catalytic performance.[53] A mimic of the reaction intermediate, oxanorbornene, was used as the organic structure directing agent (OSDA) to synthesise the DS-ITQ-2 zeolite (Fig. 4a and b).[53,54] The resultant zeolite has the MWW structure with hemi-cavities, which can stabilise the reaction intermediate, oxanorbornene, due to the pore confinement effect, and thus the DA cyclodimerization is greatly enhanced. This was further demonstrated by DFT calculations which show that the stabilisation energies of the reaction intermediates over DS-ITQ-2 are higher than those over the BEA and FAU zeolites (−82 *vs.* −66 and −50 kJ mol^{-1}, respectively, Fig. 4b–d).[53]
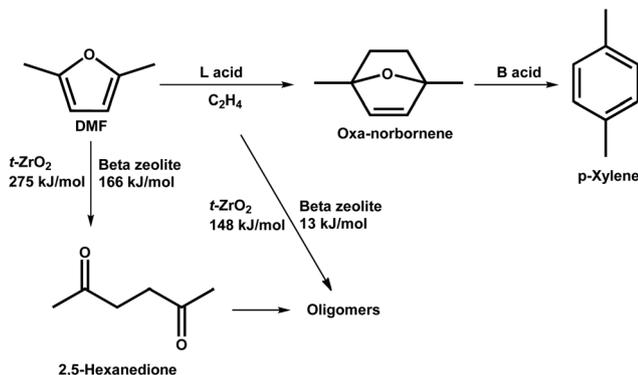
Bio-derived ethanol has been used to generate ethene *in situ* over zeolite catalysts and this renders the production of renewable aromatics notably straightforward.[57] In the ethene/DMF system, DMF is firstly protonated by Brønsted acid sites, followed by DA cycloaddition on Lewis acid sites with ethene. In the ethanol/DMF system, it was observed by SXPD that ethanol can be protonated by Brønsted acid sites of the zeolite more easily than DMF (Fig. 4e). The protonated ethanol undergoes dehydration to release ethene as a dienophile and a protonated water molecule (hydronium ion, H_3O^+). The latter

11274 | *Chem. Soc. Rev.*, 2021, **50**, 11270–11292

This journal is © The Royal Society of Chemistry 2021

Fig. 3 Conversion of lignin to aromatics. (a) Calculated energies for disassociation of the C–O bonds of phenol upon adsorption over Nb$_2$O$_5$, ZrO$_2$, Al$_2$O$_3$ and TiO$_2$. (b) Views of the corresponding DFT-optimised structural models for phenoxide bound on the Nb$_2$O$_5$(001), ZrO$_2$(010), Al$_2$O$_3$(110) and TiO$_2$(101) surfaces. Adapted from ref. 34 published by Springer Nature, licensed under a Creative Commons Attribution 4.0 International License (https://creativecommons.org/licenses/by/40/legalcode). (c) Possible reaction mechanism in the conversion of biphenyl over the Ru/NbOPO$_4$ catalyst. Inelastic neutron scattering (INS) spectra for Ru/NbOPO$_4$ in the adsorption and catalytic conversion of biphenyl. All spectra shown here are difference spectra. (d) Comparison of INS spectra for solid and adsorbed biphenyl on Ru/NbOPO$_4$. INS spectra for Ru/NbOPO$_4$ during the first (e) and second (f) catalytic conversion of biphenyl. (g) Views of selected C–C vibration modes of biphenyl. Reproduced with permission from ref. 35, Copyright© 2019 Elsevier.

This journal is © The Royal Society of Chemistry 2021

Chem. Soc. Rev., 2021, 50, 11270–11292 | 11275

Scheme 2 Reaction network of dehydrative aromatization of DMF with ethylene. Reproduced with permission from ref. 52, Copyright© 2019 Elsevier.

interacts with ethene and DMF through hydrogen bonds to form a particular configuration (Fig. 4f) that is close to the Diels–Alder transition state (Fig. 4g), resulting in a decreased activation barrier of the ethanol path by 11.2 kJ mol^{-1} as compared to the ethene route. Thus, the promoted protonation of ethanol is a key step to enhance the production of aromatics from bio-derived ethanol and DMF.

In summary, the limiting step in the production of aromatics from DMF is DA cycloaddition, which can be promoted in suitable cavities of porous catalysts due to the stabilisation of the reaction intermediates. The hydronium ion, H_3O^+, is also helpful for the stabilisation of the reaction intermediate. Both Lewis and Brønsted acid sites are involved during the transformation and their cooperation is essential to achieve high catalytic performance. Catalysts incorporating weak acid sites show clear advantages of preventing the formation of by-products.

2.2. Production of lower olefins

Olefins can be produced from biomass through pyrolysis of lignocellulose to bio-oils which include ketones, aldehydes, alcohols, esters, ethers, sugars, carboxylic acids, phenols and furans, followed by catalytic cracking processes at elevated temperatures (typically > 873 K).[58] This route, however, is highly energy-intensive and non-selective. An alternative route is to convert cellulose and hemicellulose from agricultural waste to gamma-valerolactone (GVL) via low-cost and high-yield commercialised processes.[59] GVL then undergoes ring-opening and decarboxylation to produce olefins under mild conditions.[60] GVL obtained from biorefineries is usually in 20–40 wt% aqueous solution. The conversion of GVL to olefins in water is the key step to bridge biomass and petroleum processing[61] and thus has attracted much attention. A series of solid acids including SiO_2/Al_2O_3,[60] $\gamma\text{-}Al_2O_3$,[62] La/ZSM-5,[63] Zn-AlPO-5,[64] and Pd/Nb_2O_5[65] were reported as catalysts for the conversion of GVL to butenes. However, most catalysts partially or completely lose activity in water owing to the reaction between water and Lewis acid sites. Recently, quantitative production of butenes from GVL in aqueous solution was achieved over a new heteroatomic zeolite, NbAlS-1,[36,66] which was synthesised by incorporating both Nb(v) and Al(III) centres into the MFI-type framework.

A combination of XAS, SXPD, INS and DFT has successfully revealed the reaction mechanism of the ring-opening and decarboxylation of GVL over the NbAlS-1 zeolite.[36] On HZSM-5 (an isostructural analogue to NbAlS-1 but without Nb sites), GVL adsorbs on the Brønsted acid sites via its C=O group[67] (Fig. 5a), while on NbS-1 (an isostructural analogue to NbAlS-1 but without Al sites), GVL adsorbs on the Nb(v) site through its intra-ring O-centre (Fig. 5b), which is confirmed by XAS. On the multifunctional NbAlS-1 zeolites, GVL interacts with a bridging O(H)-centre on the framework through its C=O group [C=O···O = 3.574(141) Å] via a weak hydrogen bond and with framework T-sites (NbO_4 moieties) via its intra-ring O-centre [Nb···OC_4 = 3.789(75) Å] (Fig. 5c), which was demonstrated by the Rietveld refinement of the SXPD data. The adsorption of GVL on NbAlS-1 in the unique "chelating" mode (Fig. 5c) significantly enhances its reactivity. Then selective cleavage of the C_4–O_1 bond and
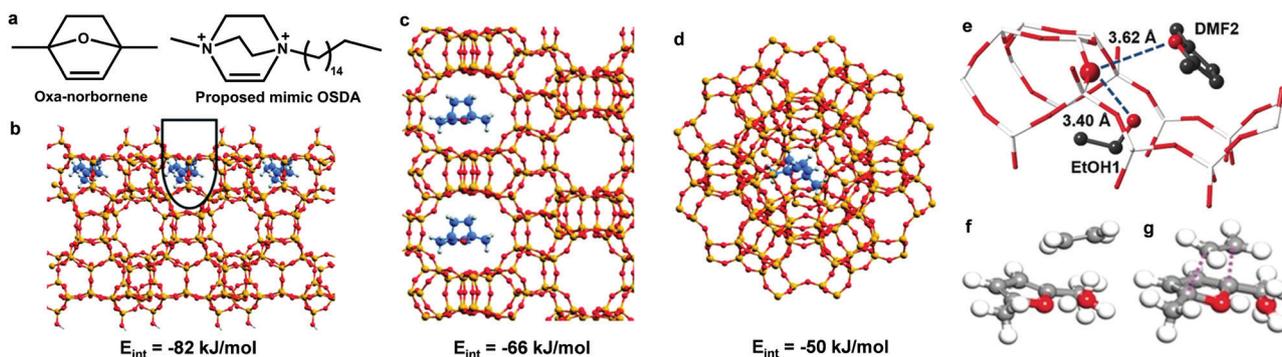

Fig. 4 Conversion of cellulose/heicellulose derivatives to aromatics. (a) Comparison of oxanorbornene and the proposed mimic organic structure directing agent. Optimised structures of the oxanorbornene intermediate in the cavities of external hemi-cavities of MWW (b) and pores of BEA (c) and FAU (d). Adapted with permission from ref. 53, published by the Royal Society of Chemistry, licensed under a Creative Commons Attribution-NonCommercial 3.0 Unported Licence (https://creativecommons.org/licenses/by-nc/3.0/). (e) Views of the crystal structure of EtOH + DMF@HZSM-5, obtained from Rietveld refinements based upon synchrotron X-ray powder diffraction data. Atoms are represented as balls/sticks: Si/Al, white; O, red (large dark red for acidic T6-OH); C, black. No hydrogen atoms are plotted. A configuration of DMF–H_3O^+–C_2H_4 (f) and the Diels–Alder transition state (g) on HZSM-5 based on DFT calculations. Grey, C; red, O; white, H. Adapted with permission from ref. 57, Copyright© 2016 John Wiley & Sons.
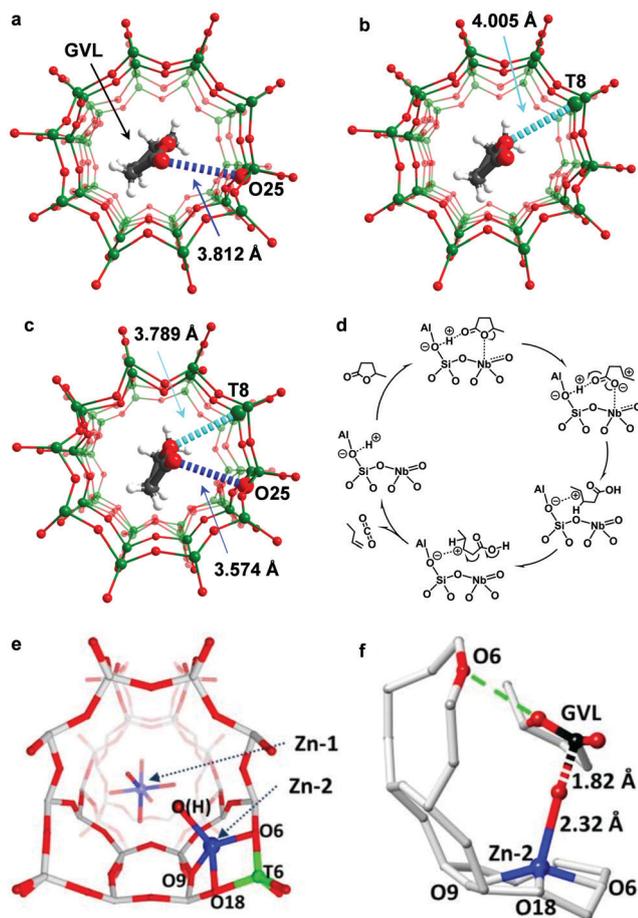
11276 | *Chem. Soc. Rev.*, 2021, **50**, 11270–11292

This journal is © The Royal Society of Chemistry 2021

Fig. 5 Production of butenes. Views of the crystal structures of GVL loaded on HZSM-5 (a), NbS-1 (b) and NbAlS-1 (c), obtained from Rietveld refinements based upon *in situ* synchrotron X-ray powder diffraction data. GVL molecules and the functional sites involved in the cooperative binding are highlighted by the use of an amplified ball-and-stick model (Nb/Al/Si, green; C, grey; O, red; H, white). The O1···Nb interactions and O2···O(H) interactions are highlighted in cyan and blue, respectively. Owing to the uncertainty in the locations of protons, all hydrogen bonds in this report are described as the distance between the O_{GVL} and the $O_{zeolite}$ centres. (d) Proposed reaction mechanisms for the conversion of GVL over NbAlS-1 based on INS/SXPD experiments. Reproduced with permission from ref. 36, Copyright© 2019 Springer Nature. Views of the crystal structures of Zn/ZSM-5 (e) and GVL loaded-Zn/ZSM-5 (f). Atoms are represented as balls/sticks: Si, grey; Al, green; Zn, blue; O, red; C, black. Adapted with permission from ref. 63, Copyright© 2017 John Wiley & Sons.

ring-opening of GVL were observed by INS due to the strong activation by Nb(v) sites. Meanwhile, $C_1=O_2$ is protonated *via* proton transfer from the Brønsted acid sites. On addition of the H-shift in the C_5-skeleton, a decarboxylation reaction *via* the cleavage of the C_1–C_2 bond occurs, yielding butene and equimolar CO_2 (Fig. 5d).

ZnO/HZSM-5 has also shown excellent catalytic performance for the ring-opening and decarboxylation of GVL.[63] SXPD, XAS and ^{1}H NMR identified that the active sites were the Brønsted acid site located at the framework T6 site[68] and a tetrahedrally coordinated Zn (Zn–OH) centre attached to the 5-membered ring of ZSM-5 through the wall-oxygens next to Al(T6)[63]

(Fig. 5e). These two sites cooperate to interact with the intra-ring O-centre [O···OC_4 = 3.34(8) Å] and C=O [Zn–O···C=O = 1.82(4) Å] group of the adsorbed GVL molecule (Fig. 5f). The activated GVL molecule then undergoes ring opening and hydrolytic decarboxylation with a water molecule to form CO_2 and 1-butene. The latter can further undergo aromatisation to produce aromatics over the ZnO/ZSM-5 catalyst.

The production of aromatics and olefins from biomass derivatives including lignin, cellulose and hemicellulose is attracting increasing attention given the demonstrated success. Based on the studies above, the key for the efficient and selective production of aromatics and olefins is to design task-specific active sites (*e.g.*, Nb site for cleavage of C–O bonds) for the activation of target chemical bonds in the substrates, and the cooperativity of different types of active sites within the microenvironment also plays an important role in achieving the unique geometry of adsorbed substrates, promoting their selective conversion.

3. Reaction mechanism for the production of bio-plastic precursors

Plastic is ubiquitous and plays an indispensable role in most synthetic products sold today.[69] At present, the global production of plastics is approximately 350 million tonnes per year,[26] which is mainly derived from non-renewable petrochemical resources. The production process of plastics causes an enormous amount of CO_2 emission. In addition, over 80 million tonnes of used plastic materials are burned, buried, or disposed of in the ocean, leading to serious problems for the environment and ecological systems owing to their high resistance to biological degradation processes.[69] It is a matter of great urgency to develop new recycling concepts,[70] clean incineration methods, and rapidly degradable plastics[71–81] to resolve these problems. The production of biodegradable plastics from renewable biomass resources can alleviate the dual pressures of shortage of petrochemical resources and environmental pollution and is therefore of great significance to the development of a sustainable society.

3.1. Production of lactic acid

Polylactic acid is a polymer synthesised from lactic acid and a new type of biodegradable material based on biomass.[74] It can be used as packaging materials, fibres and textiles, and thus has a wide range of applications in the fields of clothing and various industries (*e.g.*, construction, agriculture, forestry, and papermaking). The global production of the monomer of lactic acid is *ca.* 360 000 tonnes every year *via* both fossil and biomass resources.[82]

Owing to the abundant functional groups in biomass components, it is promising to transform them directly to target chemicals, rather than to fully decompose them, followed by the re-introduction of functional groups. A functionality index (F/C) has been introduced to guide the production of chemicals from biomass, where C is the number of carbon atoms in the

This journal is © The Royal Society of Chemistry 2021

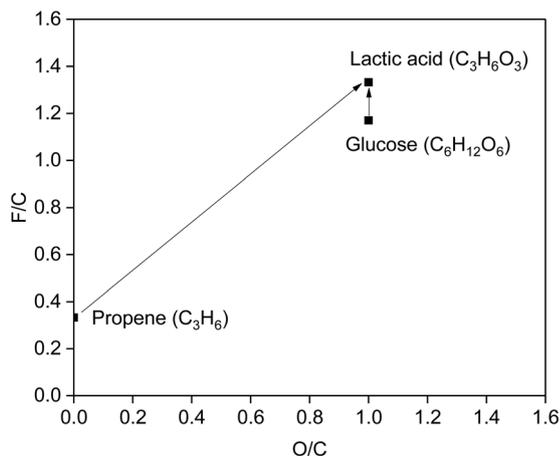*Chem. Soc. Rev.*, 2021, **50**, 11270–11292 | **11277**

Fig. 6 F/C vs. O/C ratio for propene, lactic acid and glucose. F/C refers to the functionality index, where C is the number of carbons in the molecule and F is the functionality parameter. A change of O/C indicates input or output of O to the molecule, where O and C are the number of oxygens and carbons in the molecule.

molecule and F is the functionality parameter [$F_{(C=C)} = 1$, $F_{(-OH)} = 1$, $F_{(C=O)} = 2$].[83] Besides, the atom economy is an important index in green chemistry. The change of O/C means input or output of O to the molecule (O and C are the number of oxygen and carbon atoms in the molecule), which is related to the atom economy. The plot of the F/C vs. the O/C ratio (Fig. 6) compares the production of lactic acid from biomass and fossil resources. The F/C and O/C values for lactic acid are 1.33 and 1.00, respectively. If lactic acid is obtained from fossil resources, such as C_3H_6, which has an F/C of only 0.33, functional groups with high F/C, such as –COOH and –OH, must be introduced. In contrast, biomass saccharides are intrinsically functionalised, such as glucose ($F/C = 1.17$, close to the F/C of lactic acid), which are ideal candidates to be transformed to lactic acid. Moreover, the transformation of saccharides with $C_6H_{12}O_6$ units to lactic acid has an atom economy of 100%, demonstrating the great promise of the development of biomass-based routes to produce lactic acid from saccharides.

Fermentation of edible biomass to lactic acid has been commercialised for decades.[84,85] However, biological fermentation methods suffer from long cycles and are labour-intensive. Moreover, pH buffering with an alkali during the fermentation results in producing dilute Ca-lactate salt in water. As a result, large quantities of solid waste of $CaSO_4$ (1.0 tonne per tonne of lactic acid) are produced to release lactic acid from this salt by acidification with H_2SO_4. Moreover, complex separation and purification steps are required to obtain pure lactic acid from the fermentation living broth. These drawbacks result in high production cost and low efficiency, which hamper the megatonne-scale production of polylactic acid as a commodity plastic. Thus, the development of cheap, efficient and clean catalytic technology to produce lactic acid in large quantities from inedible biomass attracts increasing attention.

The chemical conversion of saccharides to lactic acid involves cascade reactions, including hydrolysis of polysaccharides to monosaccharides, isome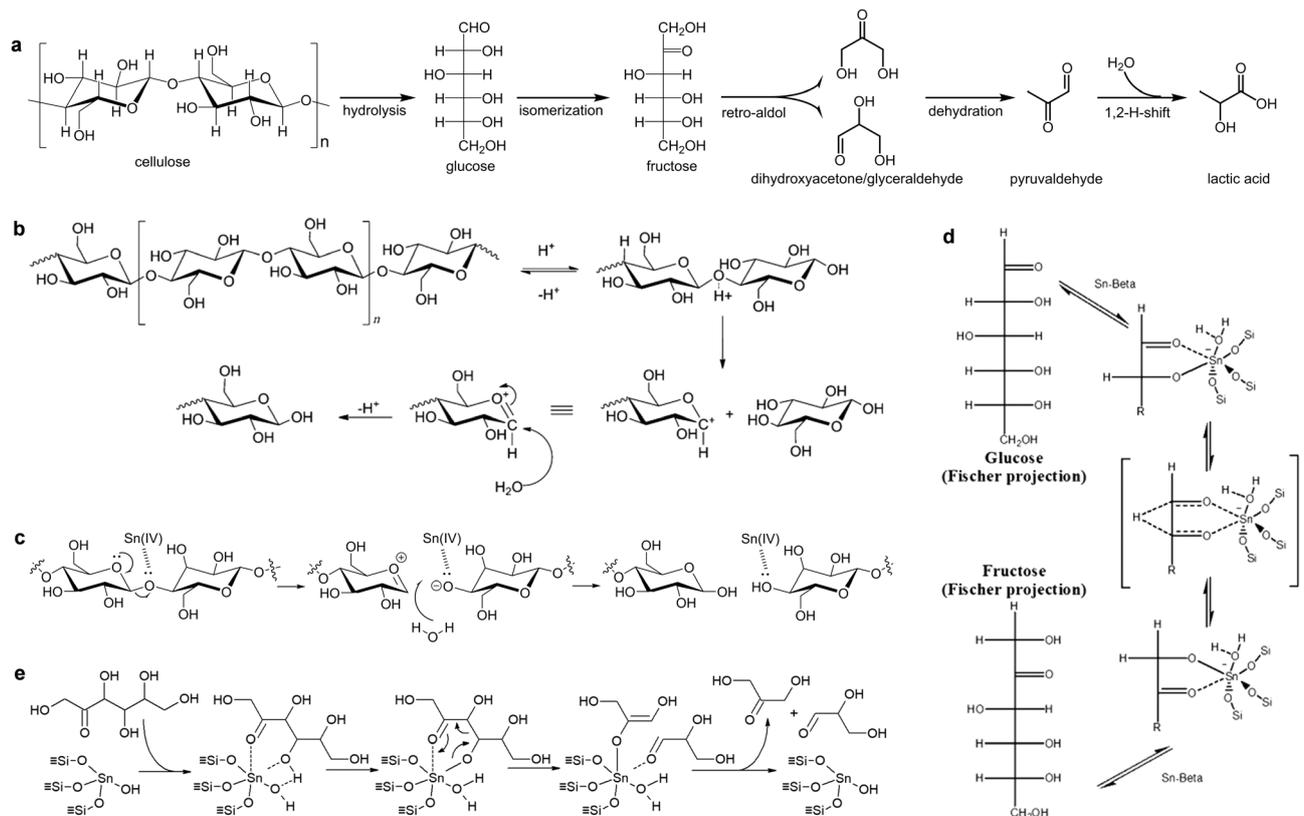risation of monosaccharides to fructose, retro-aldol condensation, dehydration, and hydride shift (Scheme 3a). Homogeneous catalysts, such as alkalis,[86] $Pb(NO_3)_2$,[87] and $Er(OTf)_3$,[88] exhibit high efficiency (up to 96% yield) to produce lactic acid (Table 1). However, it has the same drawbacks as the fermentation process due to the complex separation and purification steps. Heterogeneous catalysts such as $AlZrO_x$[89] and $AlWO_x$[90] were investigated but showed low yield (<35%) of lactic acid (Table 1).

A major breakthrough in the conversion of saccharides to lactic acid over heterogeneous catalysts was achieved by using Sn-beta zeolite, which is remarkably efficient to convert sucrose to methyl lactate (Table 1, yield 64%) at 433 K in methanol.[72] For comparison, H–Al-beta (Brønsted acidic), Ti- and Zr-beta (Lewis acidic) and Si-beta (non-acidic) were also investigated.[72] H–Al-Beta converts sugars in methanol to hydroxymethylfurfural (derivatives, methyl levulinate and methyl-D-pyranoside through dehydration. Zr-Beta and Ti-beta with weak Lewis acidity produce only moderate yields (31–44%) of methyl lactate. The non-acidic Si-beta has limited ability to produce methyl lactate (<10%). Other Sn-based zeolites such as Sn-MWW also exhibit similar catalytic performance (Table 1).[91] These results indicate that the Sn sites on the zeolite play a key role in the production of methyl lactate. A large amount of efforts were devoted to studying the reaction mechanism over Sn-zeolites to understand their high catalytic performance. Isotopic labelling, NMR spectroscopy and DFT calculations were employed to investigate the catalytic processes including hydrolysis, isomerisation, retro-aldol condensation, hydride shift and dehydration, which are discussed below.

Hydrolysis. Hydrolysis of polysaccharides or disaccharides into monosaccharides can be catalysed by both Brønsted and Lewis acids.[92] The Sn-beta zeolite has moderate Brønsted acidity which arises from structural defects (Si–OH groups).[93] It has been reported that the H^+ ions generated by hot water can also catalyse hydrolysis reactions.[94] Thus, in this system, the active sites may be Lewis acids originating from Sn(IV) sites and Brønsted acids arising from Si–OH or hot water. On the Brønsted acid site, one β-1,4-glycosidic linkage in the polysaccharide is protonated and decomposes to one molecule of glucose and one oxocarbonium ion.[95] Then the water reacts with the latter to form a terminal glucose unit accompanied by the release of one proton (Scheme 3b). On the Lewis acid site, the oxygen atom of the β-1,4-glycosidic linkage is coordinated to a Sn(IV) site, thus promoting its cleavage, which is followed by the reaction with water to form terminal glucose units (Scheme 3c).[92,96]

Isomerisation. The initial step in the isomerisation of glucose to fructose involves the ring opening of a glucose molecule. Subsequently, a hydroxyl bound to Sn(IV) results in the deprotonation of the O-2 centre. In the meantime, Sn(IV) sites withdraw electron density from carbonyl moieties in glucose to form a 5-member bidentate complex, resulting in a partial positive character at the C-1 centre (Scheme 3d), which then promotes the hydride shift from C-2 to C-1. This intramolecular hydride shift was confirmed by ^1H and ^{13}C NMR spectroscopy on isotopically labelled glucose.[97] Finally, the

Scheme 3 Production of lactic acid. (a) Reaction pathway of cellulose to lactic acid. (b) Proposed reaction mechanism for the hydrolysis of cellulose over a Brønsted acid. Reproduced with permission from ref. 95, Copyright© 2011 John Wiley & Sons. (c) Proposed reaction mechanism for the hydrolysis of cellulose over a Lewis acid. Adapted with permission from ref. 96, Copyright© 2007 Elsevier. (d) Glucose isomerization mechanisms by way of intramolecular hydride shift over Sn-beta zeolite. Adapted with permission from ref. 97. Copyright© 2011 John Wiley & Sons. (e) Plausible mechanisms for retro-aldol condensation of fructose to dihydroxyacetone and glyceraldehyde, catalysed by open tin sites. Adapted with permission from ref. 26 and 100, Copyright© 2018 John Wiley & Sons.

protonated hydroxyl group on the Sn(IV) sites releases the proton to O-1, yielding the α-hydroxy ketone. The activation energy of glucose isomerisation on Sn-beta zeolites is ~88 kJ mol^{-1} and this reaction can be achieved under mild conditions (343–413 K).[98,99] Computational studies of glucose–fructose isomerisation reveal that the ring opening of cyclic glucose suffers almost nil apparent activation barriers, while it is the intramolecular hydride shift that requires significant activation and is the rate-determining step.[99]

Retro-aldol condensation. Retro-aldol reaction, the reverse reaction of the aldol reaction, proceeds by decomposing a β-hydroxy carbonyl compound into an aldehyde or ketone and another carbonyl compound. Thus, the isomerisation of glucose to fructose prior to the retro-aldol reaction is an essential step. Carbonyl and β-hydroxy in fructose coordinate with Sn(IV) sites to form a bidentate complex (Scheme 3e). The Lewis acidic Sn(IV) sites polarise fructose by attracting electrons from the carbonyl, which promotes the scission of the C_3–C_4 bond and results in the formation of dihydroxyacetone (DHA) and glyceraldehyde (GLY).[26,100] The activation energy of retro-aldol condensation over Sn-beta is 119 kJ mol^{-1}.[101] During the overall conversion of glucose to lactic acid, the rate-determining step is the retro-aldol condensation. Recently, it has been reported that acid–base bifunctional sites could promote the retro-aldol condensation as the carbonyl and hydroxyl groups in fructose can be simultaneously activated by a Lewis acid and base, respectively.[102,103]

The two retro-aldol products, dihydroxyacetone (DHA) and glyceraldehyde (GLY), are interconvertible through intra-molecular hydride shift.[104] They can be converted easily to lactic acid (activation energies of 58–88 kJ mol^{-1}) through dehydration over Lewis or Brønsted acid sites, hydride shift over Lewis acid sites and rehydration over Brønsted acid sites under mild reaction conditions (353–398 K).[104–108]

Compared with fermentation processes, the selectivity on the Sn-beta system is lower (Table 2). A series of Sn-based zeolites have been prepared and investigated, such as Zn–Sn-beta and Pb–Sn-beta (LA 48% and 52%),[109] hierarchical Sn-beta (methyl LA 58%),[110] nanosize Sn-beta (methyl LA 57%),[111] Sn-beta + K$_2$CO$_3$ (methyl LA 72%),[112] Sn-MCM-41 COOH (methyl LA 45%),[113] and Sn-MFI + MoO$_3$ (ethyl LA 66%),[114] as well as other catalysts, such as Zr-SBA-15 (ethyl LA 33%),[115,116] Ga-doped Zn/H-nanozeolite Y catalysts (methyl LA 58%),[117] and Er-exchanged montmorillonite K10 (LA 68%).[118] The yield of lactic acid or methyl lactate was improved to 72% in the system of Sn-beta + K$_2$CO$_3$,[112] but it is still lower than that achieved by

This journal is © The Royal Society of Chemistry 2021

Chem. Soc. Rev., 2021, **50**, 11270–11292 | 11279

Table 1 Summary of typical homogeneous and heterogeneous catalysts for conversion of saccharides to lactic acid or methyl lactate

Catalysts	Substrate	Reaction conditions	Conv (%)	LA/methyl lactate yield (%)	Ref.
$Ba(OH)_2$	Glucose	298 K, 48 h, H_2O	99.5	95.4 (LA)	86
$Ba(OH)_2$	Fructose	298 K, 48 h, H_2O	98.7	83.5 (LA)	86
$Ba(OH)_2$	Cellulose	298 K, 48 h, H_2O	—	42.2 (LA)	86
$Pb(NO_3)_2$	Glucose	463 K, 4 h, H_2O	100	62 (LA)	87
$Pb(NO_3)_2$	Fructose	463 K, 4 h, H_2O	100	74 (LA)	87
$Pb(NO_3)_2$	Cellulose	463 K, 4 h, H_2O	100	68 (LA)	87
$Er(OTf)_3$	Glucose	513 K, 0.5 h, H_2O	100	47 (LA)	88
$Er(OTf)_3$	Fructose	513 K, 0.5 h, H_2O	100	55 (LA)	88
$Er(OTf)_3$	Cellulose	513 K, 0.5 h, H_2O	100	61 (LA)	88
$AlZrO_x$	Glucose	453 K, 2 h, H_2O	92	34 (LA)	89
$AlWO_x$	Cellulose	463 K, 24 h, H_2O	47	28 (LA)	90
Sn-Beta	Glucose	433, 20 h, MeOH	99	43	72
Sn-Beta	Fructose	433, 20 h, MeOH	99	44	72
Sn-Beta	Sucrose	433, 20 h, MeOH	100	64 (methyl lactate)	72
H–Al-Beta	Sucrose	433, 20 h, MeOH	99	0	72
Ti-Beta	Sucrose	433, 20 h, MeOH	98	44 (methyl lactate)	72
Zr-Beta	Sucrose	433, 20 h, MeOH	99	40 (methyl lactate)	72
Sn-MWW	Glucose	433, 20 h, MeOH	99	44 (methyl lactate)	91
Sn-MWW	Fructose	433, 20 h, MeOH	99	46 (methyl lactate)	91
Sn-MWW	Sucrose	433, 20 h, MeOH	99	50 (methyl lactate)	91

the fermentation process (95%, Table 2). Therefore, we summarise the reaction network including the details of active sites, reaction temperatures and activation energies (Scheme 4) to inform the design of new efficient catalysts. Among the conversion of cellulose to lactic acid, hydrolysis and dehydration can be catalysed by both Brønsted and Lewis acid sites, and the former has higher reactivity. Isomerisation, retro-aldol, and 1,2-H-shift can readily occur on Lewis acid sites. The formation of by-products such as 5-hydroxymethylfurfural (5-HMF) and humins mainly occurs on Brønsted acid sites. Thus, the decrease of Brønsted acid sites would significantly hinder the formation of by-products. This was confirmed by a study which shows that the selectivity of lactic acid can be improved by decreasing the ratio of Brønsted/Lewis acid sites.[119] Although the hydrolysis of cellulose and dehydration of GLY can be affected in the meantime, it would have little effect on the overall reaction, because the rate-determining step is the retro-aldol reaction (the activation energy on Sn-beta is 119 kJ mol^{-1}). Moreover, the accumulation of glucose from cellulose via hydrolysis can promote the formation of by-products, such as erythrose and glycolaldehyde. Thus, a slight reduction of the hydrolysis in turn is beneficial for improving the yield of lactic acid. Although the

retro-aldol reaction of saccharides on Sn-beta zeolites occurs predominantly from fructose rather than glucose,[100] the latter accounts for 10%, which needs further strategies to reduce the retro-aldol reaction of glucose. In conclusion, four aspects need to be considered to design an efficient catalyst: (i) controlling precisely the Brønsted acid sites in order to adjust the hydrolysis reaction and to selectively reduce the formation of 5-HMF and humins; (ii) developing new strategies to promote the retro-aldol cleavage between C_3 and C_4 centres and to hinder other retro-aldol reactions; (iii) discovering suitable Lewis acid sites to operate under mild reaction conditions and hence to reduce side reactions; and (iv) designing porous structures of the catalyst to improve the mass transfer of the reactants, intermediates and products.
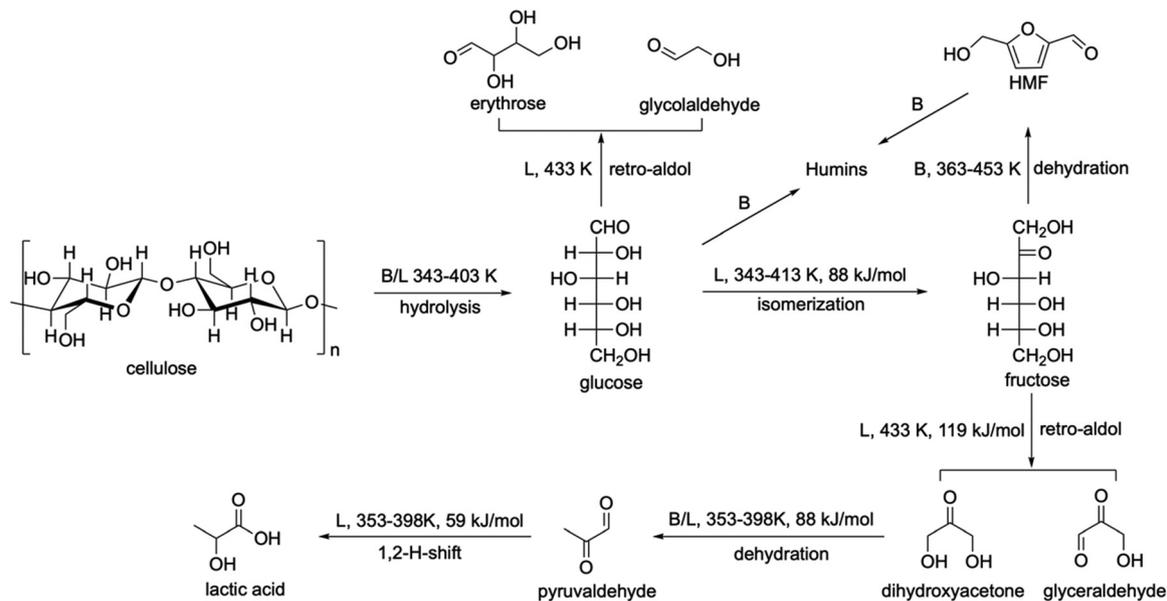
3.2. Production of 2,5-furandicarboxylic acid (FDCA)

FDCA is a precursor to produce sustainable polymers, such as polyethylene 2,5-furandicarboxylate, which can replace the petroleum-derived polyethylene terephthalate.[120] The conversion of fructose to FDCA undergoes two steps: dehydration of fructose to 5-HMF and oxidation of 5-HMF to FDCA. Heterogeneous catalysts based upon noble metals, such as Pt, Au, Ru and Pd

Table 2 Comparison of heterogeneous catalytic routes vs. classic (bacterial) fermentation. Reproduced with permission from ref. 105, Copyright© 2014 Springer Nature

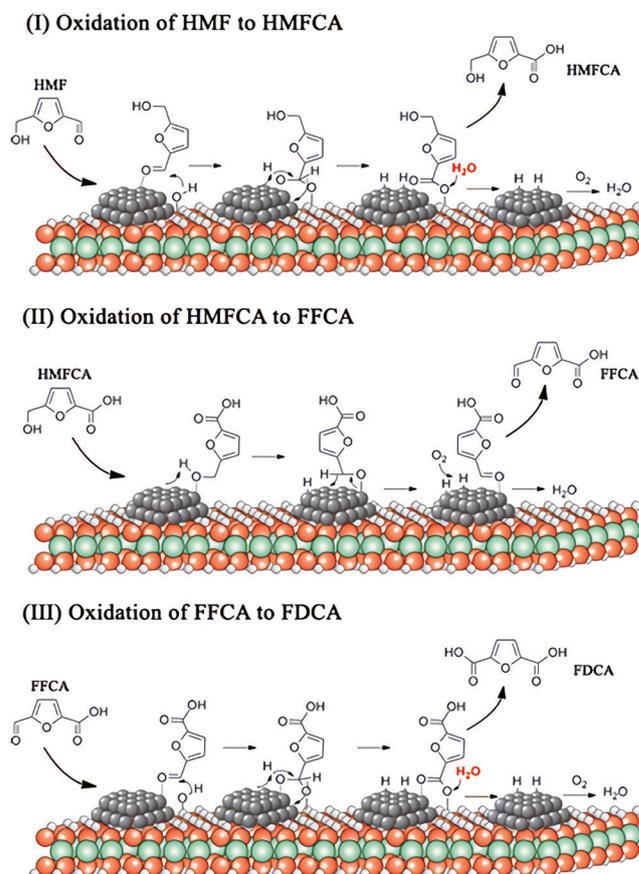| Criterion	Heterogeneous[72]	Fermentation[84,85]
Media	Alcohol	Aqueous broth
Feedstock	Glucose, sucrose	Glucose, sucrose
Concentration feed	Up to 10 wt%	Up to 15 wt%
Catalyst	Sn-Beta zeolite	Bacteria (yeast)
Co-reagents	None	Alkali + nutrients
Major product	Alkyl lactates	Ca-lactate salt
Stereopurity product	Racemic	L
Selectivity (mol%)	Up to 64%	Up to 95%
Productivity	Up to 3.3 g $L_{reactor}^{-1}$ h^{-1}	0.3–5 g $L_{reactor}^{-1}$ h^{-1}
Gypsum co-product	No	1 kg per kg of LA
Work-up	Easy: filtration, distillation, alcohol reuse	Complex: acidification, two filtrations, purification, esterification, distillation
Catalyst reuse	Yes	No (in a complex broth)

Scheme 4 Summary of the main and side reactions during the conversion of cellulose to lactic acid. B and L represent Brønsted and Lewis acid sites, respectively.

nanoparticles, combined with homogeneous base catalysts have been studied for the oxidation of 5-HMF to FDCA.[121] These catalytic systems show excellent catalytic performance with a >99% yield of FDCA under mild conditions. However, homogeneous catalysts cause serious corrosion of the equipment and can hardly be separated or recycled. A homogeneous base-free route for the oxidation of 5-HMF to FDCA by using Mg–Al–CO$_3$ hydrotalcite-supported Pd nanoparticles as the catalyst has been developed, achieving yields of FDCA of >99% at 373 K under ambient pressure.[122] The excellent catalytic performance of Mg–Al–CO$_3$ hydrotalcite-supported Pd nanoparticles under homogeneous base free-conditions is attributed to their suitable basicity and abundant –OH groups on the surface.

The reaction mechanism of aerobic oxidation of 5-HMF to FDCA over Mg–Al–CO$_3$ hydrotalcite-support Pd catalysts is proposed (Fig. 7).[122] In the first step, the aldehyde group of 5-HMF adsorbs onto the surface of Pd nanoparticles, followed by nucleophilic addition of a hydroxyl group from hydrotalcite to form a new hydroxyl group on active Pd sites. The formed hydroxyl group and C–H group are then dehydrogenated to form a carboxylic group, leaving two hydrogen atoms on the surface of the Pd nanoparticles. Then, 5-hydroxymethyl-2-furancarboxylic acid (HMFCA) is produced through a hydrolysis reaction, accompanied by regeneration of the hydroxyl group on hydrotalcite. The H atoms on the Pd nanoparticles react with O$_2$ to form peroxide and water. In the second step, the hydroxymethyl group in HMFCA adsorbs onto the surface of the Pd nanoparticles, and O–H and C–H bonds are activated, followed by an elimination reaction of β-hydride to generate 5-formyl-2-furancarboxylic acid (FFCA). In the same way as the first step, the carbonyl group of FFCA is oxidised to FDCA.

The proposed reaction mechanism reveals that the cooperativity between noble metals and basic sites of the support is of critical

Fig. 7 View of the plausible reaction mechanism of oxidation of 5-HMF to FDCA over Pd/HT catalysts. Reprinted with permission from ref. 122, Copyright© 2016 American Chemical Society.

This journal is © The Royal Society of Chemistry 2021

Chem. Soc. Rev., 2021, **50**, 11270–11292 | **11281**

importance for the oxidation of 5-HMF to FDCA. Future improved catalysts need to be ideally based upon earth-abundant metals, which can retain synergistic effects with basic supports. The low yield of 5-HMF from the conversion of fructose is another major barrier to the production of FDCA from biomass, and this is discussed below.

4. Reaction mechanism for the production of liquid fuels

Conversion of biomass to liquid fuels is considered as less appealing than to bulk chemicals in terms of added value per tonne of biomass ($200–400 *vs.* ~$1000 for liquid fuels and chemicals, respectively).[123] However, the sum of demand for liquid fuels is significantly higher than for bulk chemicals. For example, ~90% of crude oil is consumed as fuels while only the remaining 10% is upgraded to chemicals. Thus, the synthesis of sustainable fuels represents an enormous market in the conversion of biomass. First-generation biodiesel and bioethanol are manufactured from edible plant crops, which competes with food production in terms of land use.[1] Therefore, the conversion of inedible lignocellulosic biomass to fuels represents a target sustainable approach.[7,35,124–127] The strategy that breaks down lignocellulosic biomass to syngas $(CO + H_2)$ through gasification, followed by the Fischer–Tropsch process to upgrade the syngas to alkanes, is effective but energy-intensive. Alternatively, through liquefaction, hydrolysis, or dehydroxygenation, lignocellulosic biomass can be converted to liquid fuels, such as alkanes, aromatic hydrocarbons or other small molecules.[128–130]

4.1. Conversion of fructose to DMF

DMF has a suitable boiling point (366 K), low water solubility (2.3 g L^{-1}), high research octane number (119) and high energy density (30 kJ cm^{-1}), which make it an ideal candidate as liquid fuel for transportation.[126] A two-step route to convert fructose to DMF has been reported.[126] In the first step, fructose is transformed to 5-HMF through dehydration in an HCl/NaCl/solvent/water system at 180 °C with a 5-HMF yield of 70%. After separation and purification, in the second step, 5-HMF is converted to DMF (yield 76%) on a CuRu/C catalyst *via* hydrogenation and HDO at 220 °C. The reaction mechanisms of dehydration, hydrogenation and HDO over these solid catalysts were studied by the isotope-labelling technique and NMR spectroscopy.

Dehydration. The direct dehydration of fructose to 5-HMF could proceed *via* either the acyclic[131] or cyclic pathway.[29,132] The acyclic pathway is however ruled out by deuterium labelling experiments, and the cyclic route was proposed by employing ^{13}C, ^{1}H and ^{17}O isotope-labelling techniques and NMR spectroscopy.[29] Fructose and its isomers are present (slowly reaching equilibrium at low temperature) where O2–H in fructose in the ring form is protonated. O2–H in fructose is demonstrated to have the highest proton affinity.[133] Thus, the first dehydration occurs on this site, leading to the formation of

fructosyl oxocarbenium ions (Scheme 5a). This active intermediate quickly deprotonates to transform to 3,4-diol, followed by consecutive dehydration to yield 5-HMF. By-products may also originate from the active intermediate fructosyl oxocarbenium ions. Reversible intramolecular or intermolecular nucleophilic attack of oxocarbenium ions by the hydroxyl group followed by deprotonation leads to the formation of 2,6-anhydro-β-D-fructofuranose or difructose-dianhydrides, respectively. They could then form a six-membered ring fructopyranosil oxocarbenium ion, leading to the formation of oligomers and humins.

Dimethyl sulfoxide (DMSO) has been identified as a suitable solvent for the synthesis of 5-HMF catalysed by Amberlyst 70 and it can limit side reactions. Among fructose isomers, the concentration of D-fructofuranose is significantly higher in DMSO than in other solvents such as H_2O and MeOH. The nucleophilic attack of DMSO to the fructopyranosil oxocarbenium ions forms a key intermediate [2-(hydroxydimethylsulfinyloxy)-β-D-fructofuranose] (Scheme 5b).[134] This intermediate can be readily converted to 5-HMF rather than to oligomers and humins. In addition, 5-HMF has high reactivity and can transform to humins, and, in order to avoid any further reaction of 5-HMF, a bi-phase system to extract 5-HMF from the reaction mixtures was developed.[135]
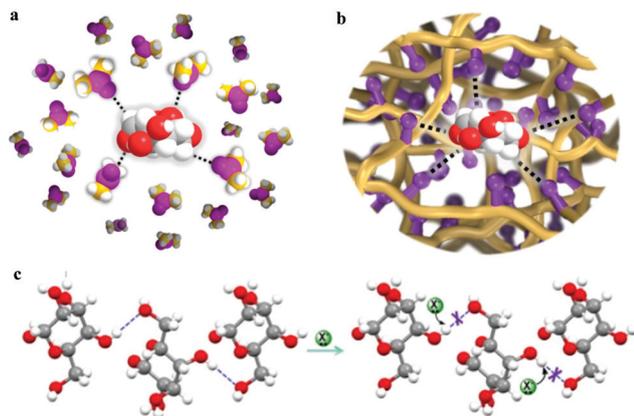
Recently, porous solid solvents (PSSs), which are comprised of solvent moieties (*i.e.*, DMSO and ionic liquids) and solid acid sites (*i.e.* sulphonic groups), have been designed for enhancing the conversion of fructose to 5-HMF.[136] The solvent moieties in PSSs as hydrogen-bond acceptors mimic liquid-phase solvents to break the hydrogen bonding network of fructose and to stabilise the intermediate (Fig. 8). Moreover, the solvent moieties surrounding the acid sites can enhance their cooperation, resulting in higher catalytic performance compared with that in liquid solvent systems. This new approach significantly improves the yield of 5-HFM in a green manner by avoiding costly separation processes.

Hydrogenation and HDO. HDO is a process to remove oxygen from oxygen-containing compounds such as biomass *via* a hydrogenolysis reaction. Conversion of 5-HMF to DMF requires hydrogenation of the –CHO groups and hydrogenolysis of the –OH groups (*i.e.*, the HDO process).[137,138] Single-metal-based catalysts, such as Ru, Pd, Pt, Cu, Ni, and Co, are active for the conversion of 5-HMF to DMF,[139] but DMF can be easily over-hydrogenated to by-products. Bimetallic catalysts such as Pt–Co, Pt–Ni, Pt–Zn, Pt–Cu, Cu–Co, Ni–Co, Cu–Ni, and Ni–Fe have been demonstrated to show excellent catalytic performance with selectivities of DMF >96%.[137,140–144]

The reaction mechanism of the conversion of 5-HMF to DMF over PtCo nanocrystals was investigated by XRD, XAS and DFT calculations.[137] XRD and XAS analysis suggests that the Pt_3Co_2 catalyst consists of a Pt-rich core (88% Pt and 12% Co) and a Co_3O_2 surface monolayer (Fig. 9a), which are responsible for the dissociation of H_2 and cleavage of C–O bonds, respectively. The first step is the dissociation of H_2, which can occur *via* homolytic and/or heterolytic dissociation paths. The homolytic splitting of H_2 molecules over Co and Pt atoms is energetically favourable, resulting in a Co–H–Pt bridging configuration.

Scheme 5 Dehydration of fructose to 5-HMF. (a) Proposed reaction mechanism of acid-catalysed dehydration of fructose to 5-HMF *via* the cyclic pathway. Reproduced with permission from ref. 29, Copyright© 2012 Royal Society of Chemistry. (b) Proposed role of DMSO in conversion of fructose to 5-HMF. Adapted with permission from ref. 134, Copyright© 2016 Elsevier.

This journal is © The Royal Society of Chemistry 2021

Chem. Soc. Rev., 2021, **50**, 11270–11292 | 11283

Fig. 8 Schematic illustration of fructose in various systems. (a) Solvent DMSO containing hydrogen bond acceptors interacting with fructose through hydrogen bonds. (b) Solvent moieties (purple) anchored on a porous solid material interacting with fructose through hydrogen bonds. (c) The interruption of the hydrogen network of fructose by solvent moieties (X^-). C in DMSO, yellow; C in fructose, grey; H, white; S, light magenta; O in DMSO, dark magenta; O in fructose, red; hydrogen bond, dash line. Reproduced from ref. 136, published by Springer Nature, licensed under a Creative Commons Attribution 4.0 International License (https://creativecommons.org/licenses/by/4.0/legalcode).
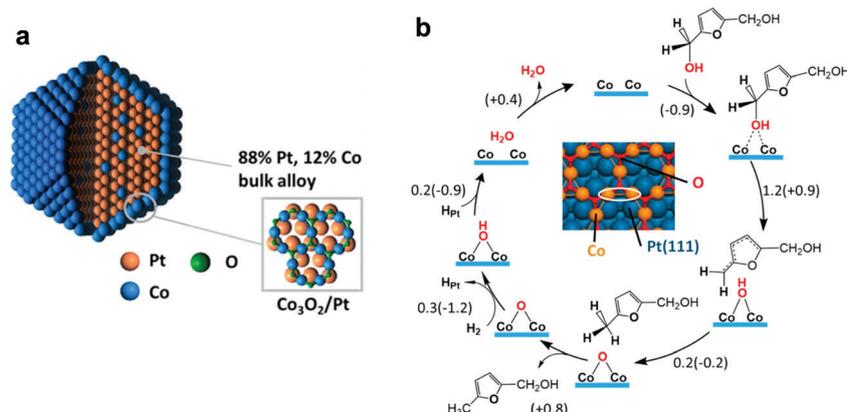
Then, the two dissociated H atoms are added to the carbonyl group of weakly adsorbed 5-HMF, yielding 2,5-bis(hydroxymethyl)furan. Subsequently, the HDO of 2,5-bis(hydroxymethyl)furan occurs on the Co_3O_2 coating (Fig. 9b). The two Co atoms break the C–O bonds to yield a loosely bound radical and an –OH group. Then, the radical moiety drags a hydrogen atom from the –OH group, yielding 2-hydroxylmethyl-5-methyl furan and a chemisorbed oxygen atom. Similarly, C–O scission on 2-hydroxylmethyl-5-methyl furan results in the formation of DMF. Finally, the chemisorbed O atom reacts with H_2 to form water and complete the catalytic cycle. The scission of the C–O bond can be catalysed over the surface layer of Co_3O_2, whereas the chemisorption of the furan ring is difficult on Co_3O_2. Thus, the ring-opening and decarboxylation of the formed DMF is hindered, leading to the selective production of DMF.

The reaction pathway described above can be altered over Pd-based N-doped mesoporous carbon (Pd/NMC) materials with the assistance of formic acid, and a high yield of DMF can be achieved (>97%, Fig. 10a).[145] In the Pd/NMC material, two pyridinic N atoms interact with one Pd atom, leading to a change in the oxidation state of Pd^0 to Pd^{2+} (Fig. 10b and c). Formic acid is activated by Pd^{2+} centres and decomposes to a formate anion and H^+ (Fig. 10d). The H^+ from formic acid protonates the C–OH group of HMF that is bound to the Pd^{2+} species, thus driving the cleavage of the C–OH bond during the hydrogenolysis of HMF to 5-methylfurfural (5-MF) with H^- from heterolytic dissociation of H_2 on Pd^0 nanoparticles. Then the –CHO group of 5-MF is hydrogenated on Pd^0, followed by a similar hydrogenolysis process on Pd^{2+} to produce DMF.[145] In this system, the synergistical cooperation of Pd^{2+} species and formic acid in the hydrogenolysis of the C–OH bond leads to the improvement of the activity,[145] and formic acid also acts as a mild hydrogen source and suppresses the ring-hydrogenation to improve the selectivity of DMF.[146–148]

Mechanism studies provide insights into the design of catalysts for the selective production of DMF from fructose, and inspire a series of studies on one-pot production of DMF from fructose.[149] A carbon-based solid functionalised with p-toluenesulfonic acid (TsOH) and an encapsulated CuCo multifunctional catalyst (CuCo@C-TsOH) can directly convert fructose to DMF with a yield of 71%.[150] Recently, a multifunctional catalyst Cu–Pd/UiO-66(NH$_2$)@SGO was developed for direct conversion of saccharides to DMF.[151] The Cu–Pd/UiO-66(NH$_2$)@SGO (SGO = sulfonated graphene oxide) catalyst, which has Brønsted acid sites, Lewis acid sites and HDO active sites, shows excellent catalytic performance for direct conversion of fructose to DMF with a yield of 85%.
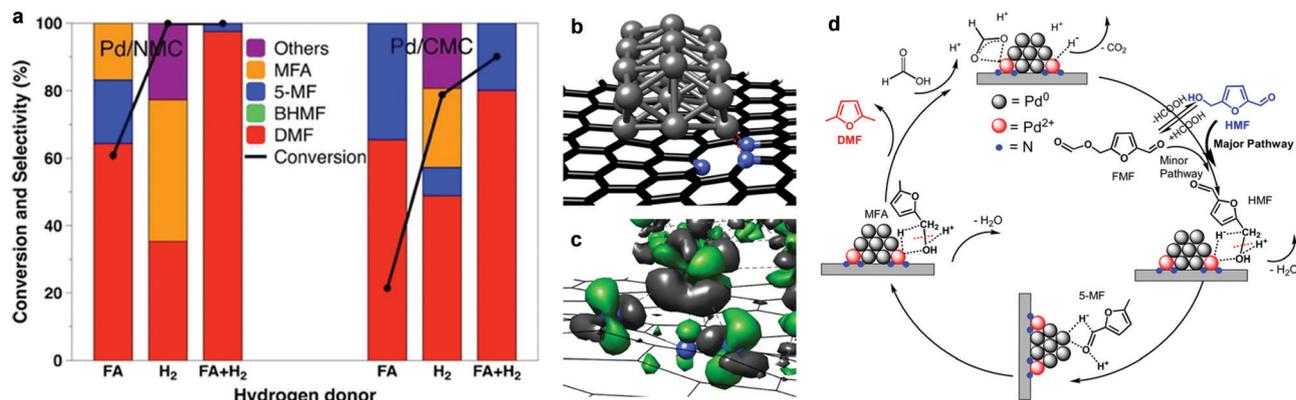
4.2. Production of C5/C6 alkanes

Production of liquid alkanes from cellulose/hemicellulose has attracted tremendous attention because C5/C6 alkanes are components of liquid fuels.[152–154] It has been demonstrated

Fig. 9 Mechanism of HDO of 5-HMF. (a) Pt$_3$Co$_2$ nanocrystal model involving an alloy core (88% Pt, 12% Co) covered with a Co_3O_2 surface oxide monolayer with a honeycomb structure. (b) Reaction mechanism of 2,5-bis(hydroxymethyl)furan hydrodeoxygenation to 2-hydroxylmethyl-5-methyl furan on the Co_3O_2/Pt(111) surface. DFT reaction barriers (energies) are given in eV. The inset depicts a portion of a Co_3O_2/Pt(111) surface. Two Co atoms participating in C–O bond activation are encircled with a white ellipsoid. Reproduced with permission from ref. 137, Copyright © 2016 American Chemical Society.
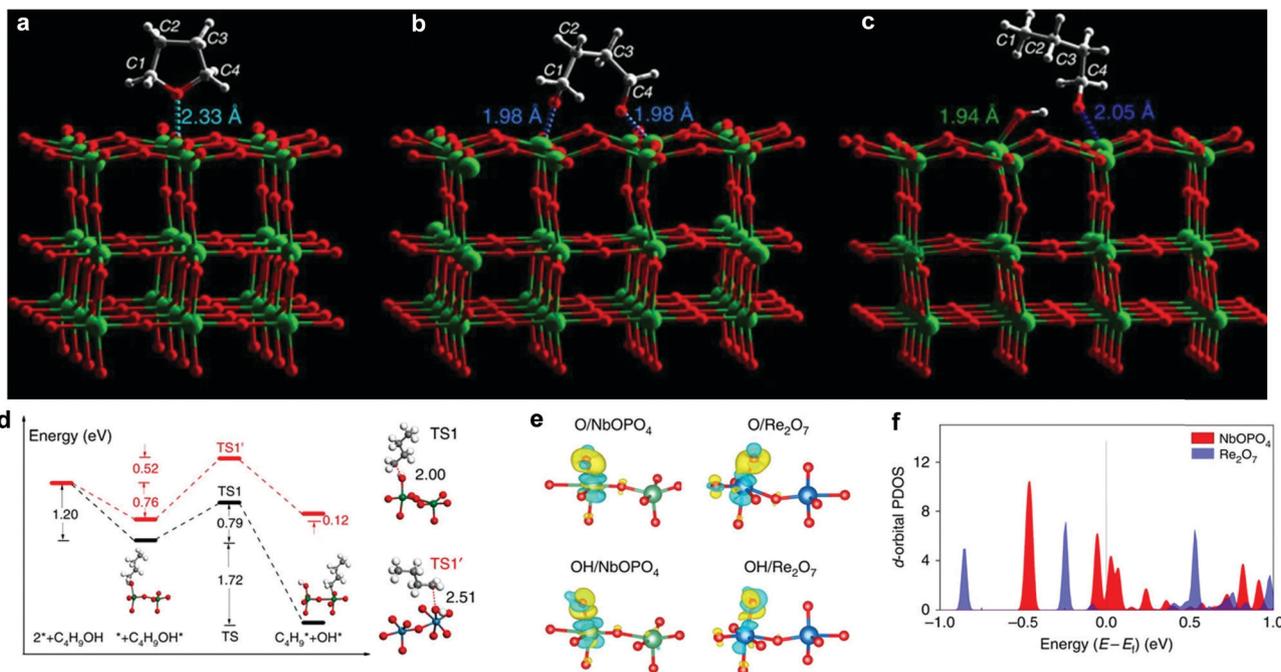
11284 | Chem. Soc. Rev., 2021, 50, 11270–11292

This journal is © The Royal Society of Chemistry 2021

Fig. 10 Conversion of HFM to DMF using different hydrogen sources over Pd-based catalysts. (a) Most stable structure of Pd21 on a pyridinic carbon support (two pyridinic N connected to Pd21) calculated for the Pd/NMC model. (b) Change in the electron density induced by the interaction between the Pd21 cluster and the pyridinic N atoms (green: density gain; grey: density loss). (c) Comparison of Pd/NMC and Pd/CMC with respect to the conversion of HMF to DMF using different hydrogen sources after 3 h. (d) Proposed reaction pathway for the conversion of HMF to DMF over Pd/NMC in FA. Reproduced from ref. 145, published by John Wiley and Sons, licensed under a Creative Commons Attribution 4.0 International License (https://creativecommons.org/licenses/by/4.0/legalcode).

that sorbitol can be transformed to C5/C6 alkanes under mild conditions in an aqueous-phase reforming process.[155] This discovery is the cornerstone to developing new processes for production of liquid fuels from biomass. By using Ir–ReO$_x$/SiO$_2$ combined with HZSM-5 as a catalyst, cellulose has been successfully converted to *n*-hexane.[156] A multifunctional Pt/NbOPO$_4$ catalyst has shown excellent catalytic performance for the direct conversion of raw woody biomass into liquid

Fig. 11 View of the optimised structural models of adsorbed THF (a), reacted (ring-opened) THF (b) and 1-butanol after adsorption to generate 1-butanoxide and surface hydroxyl (c) on the (001) plane of the catalyst Pt/Nb$_2$O$_5$ (Nb: green; O: red; C: grey; H: white). (d) Calculated energy profiles of C−O bond cleavage of C$_4$H$_9$OH. Black and red lines indicate NbOPO$_4$(100) and Re$_2$O$_7$(010), respectively. The structures of the initial and final states on NbOPO$_4$(100) are shown, whereas the transition state involving C−O bond cleavage of C$_4$H$_9$OH is depicted as TS1 and TS1′, with the elongated C−O bond lengths shown. Emerald balls represent Nb atoms, dark blue for Re, white for H, grey for C and red for O. (e) The isosurfaces of the charge density difference for O and OH adsorption on the NbOPO$_4$(100) and Re$_2$O$_7$(010) surfaces. For clarity, only the local active sites are shown. The regions depicted in yellow indicate charge accumulation and light blue for charge depletion. Emerald balls represent Nb atoms, dark blue for Re, white for H and red for O. (f) The d-orbital projected density of states for the surface Nb$_{5c}$ and Re$_{5c}$ atoms, demonstrating their relative energies, in which the energy is aligned to the Fermi level. Reproduced from ref. 7, published by Springer Nature, licensed under a Creative Commons Attribution 4.0 International License (https://creativecommons.org/licenses/by/4.0/legalcode).

This journal is © The Royal Society of Chemistry 2021

Chem. Soc. Rev., 2021, 50, 11270–11292 | 11285

alkanes,[7] where the major barrier is the ring-opening and the sequential HDO of tetrahydrofuran (THF) derivatives (*e.g.*, DMF). The reaction mechanism of key steps, *i.e.* ring-opening and HDO of THF on Pt/Nb$_2$O$_5$, were studied by INS and computational methods. Firstly, THF is adsorbed on the surface *via* interactions between its ring O($\delta-$) centre and the open Nb($\delta+$) site (O$\cdots$Nb = 2.33 Å) (Fig. 11a). The adsorbed THF molecule reacts on strong Lewis acid sites [Nb(v)], and forms an intermediate bound to two adjacent Nb(v) centres simultaneously (O$\cdots$Nb = 1.98 Å) *via* ring-opening (Fig. 11b). This intermediate is unstable, and quickly transforms to 1-butanoxide bound to the surface Nb(v) sites under H$_2$ (dissociation over Pt sites), which was observed experimentally by INS (Fig. 11c). Further cleavage of the C–O bond of 1-butanoxide on NbOPO$_4$ was investigated by first-principles calculations and the widely used ReO$_x$ catalyst in biomass conversion was also studied for comparison. Catalysed by surface Nb$_{5c}$, the C–O bond can be cleaved with only a barrier of 76.2 kJ mol^{-1}, whereas it has to overcome a larger barrier of 124 kJ mol^{-1} on Re$_2$O$_7$ (Fig. 11d). The dissociation barrier of the C–O bond was found to be related to their corresponding adsorption energies and the stronger the bond strength of M$_{5c}$–O (M = Nb, Re), the easier the C–O bond cleavage. An analysis of the electronic structure shows electron accumulation between O (or OH) and Nb$_{5c}$ (or Re$_{5c}$) (Fig. 11e), indicating a typical covalent bond character, of which the strength is determined by the size and energy level of the d-orbital of M$_{5c}$ cations. The d-orbitals of Nb$_{5c}$ near the Fermi level are more delocalised, and the energy level of the highest occupied d-bands is higher for Nb$_{5c}$ compared to Re$_{5c}$ (Fig. 11f). Thus, NbOPO$_4$ has strong binding ability and can effectively catalyse the deoxygenation reaction.

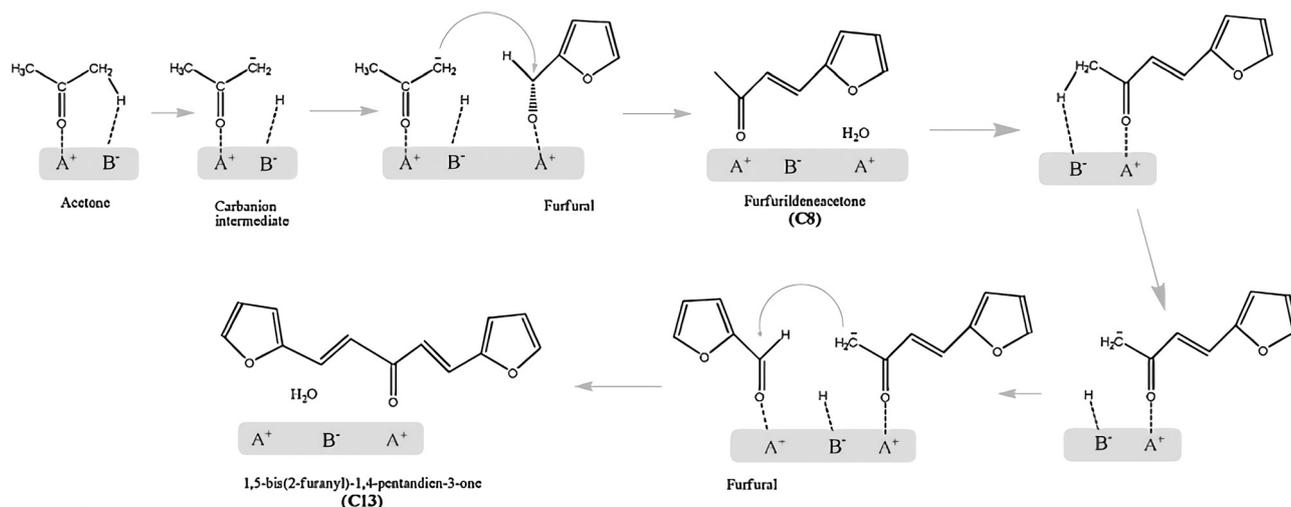### 4.3. Production of long-chain alkanes

As the boiling points of C5/C6 alkanes are low (309–342 K), production of long-chain alkanes from biomass is more desirable for direct use as gasoline. A stepwise route has been proposed to produce C7–C15 liquid alkanes.[89] It proceeds through dehydration of biomass-derived carbohydrates on acid catalysts, aldol condensation of furanic compounds with ketones to form large organic compounds on base catalysts, and HDO to form long-chain alkanes on acid/metal sites. Among these steps, the aldol condensation is the step that determines the overall number of carbon atoms and, hence, impacts the quality of the obtained fuel.

The reaction mechanism of aldol condensation of furfural-acetone on acid–base pairs is proposed in Scheme 6 based on kinetic studies.[157] Acetone firstly adsorbs on acid–base pairs and its α-proton is abstracted by base sites, resulting in the formation of a carbanion intermediate, which is stabilised by weak acid sites. The adsorbed furfural molecule on a weak acid site is then attacked by the carbanion *via* the interaction between the carbanion and carbonyl group. This step leads to the formation of an α-hydroxyl ketone which is unstable and rapidly dehydrates to C8 compounds and water, accompanied by the regeneration of active sites. Similarly, further aldol condensation of C8 compounds with furfurals produces C13 compounds. Kinetic studies indicate that the rate-determining step is the abstraction of α-protons by base sites. Thus, the basicity of the active site and the acidity of that proton are key factors affecting the aldol condensation between furanic compounds and ketones. The roles of weak acid sites are to adsorb reagents *via* carbonyl groups and to stabilise the reaction intermediates.

5. Reactions of C–O/C–C bonds in biomass

Lignocellulosic biomass is mainly constructed from C–O and C–C bonds. The conversion of lignocellulosic biomass involves numerous reactions, which can be generally classified as:

Scheme 6 Proposed reaction mechanism of furfural–acetone aldol condensation on acid–base pairs. Reproduced with permission from ref. 157, Copyright © 2011 Elsevier.

cleavage of C–O bonds, cleavage of C–C bonds, cleavage of C–O/C–C bonds, and formation of C–O and C–C bonds (Fig. 12). The heterogeneous catalysts for catalysing these reactions are summarised in Fig. 13. C–O bonds can be cleaved via either dehydration or hydrogenolysis. In the former, –OH is protonated by Brønsted acids (such as Amberlyst 70), resulting in the cleavage of the C–O bond. The hydrogenolysis of C–OH usually occurs on M^0/M^+ sites (M^0, metal in the reduced state; M^+, metal in the oxidised state). The M^0 site dissociates H_2 and the M^+ site activates C–OH, enabling the cleavage of C–O bonds. Where the C=C bond needs to be protected during hydrogenolysis, such as 5-HMF to DMF, and phenol to benzene, efforts need to be made to slow down the H_2 dissociation and/or to enhance the activation of the C–O bond. Several strategies have been reported. (i) A Pt/Co_3O_2 core/shell structure is designed, in which Pt is enriched in the core but lean in the shell. Thus, the dissociation of H_2 is reduced and hydrogenation of the C=C bond is hindered. (ii) A Pd/NMC/formic acid system is proposed. Pd sites partially exist in the divalent state due to interaction with pyridinic N centres, so the dissociation of H_2 is hindered by reducing the amount of Pd^0 sites. In the meantime, Pd^{2+} and formic acid both reduce the activation energy of C–O bonds. (iii) A Ru/Nb_2O_5 catalyst is designed, which consists of metal sites that dissociate H_2 mildly and Lewis acid sites that strongly bind to the C–O group. The strong Lewis acid and metal with a strong ability of H_2 dissociation (Pt/Nb_2O_5) are favourable for the cleavage of $C–O_{ring}$. The cleavage of the C–C bond is challenging and needs very strong acid sites. The functional groups nearby which polarise the C–C bond determine the pathway of its cleavage. Because the aromatic group can be

Fig. 12 Comparison of the reaction mechanisms of the cleavage of C–O, C–C, and C–O/C–C bonds, and the formation of C–O and C–C bonds. M^0 is the metal in the reduced state, and M^+ is the metal in the oxidised state. A^+B^- is the acid–base pair.
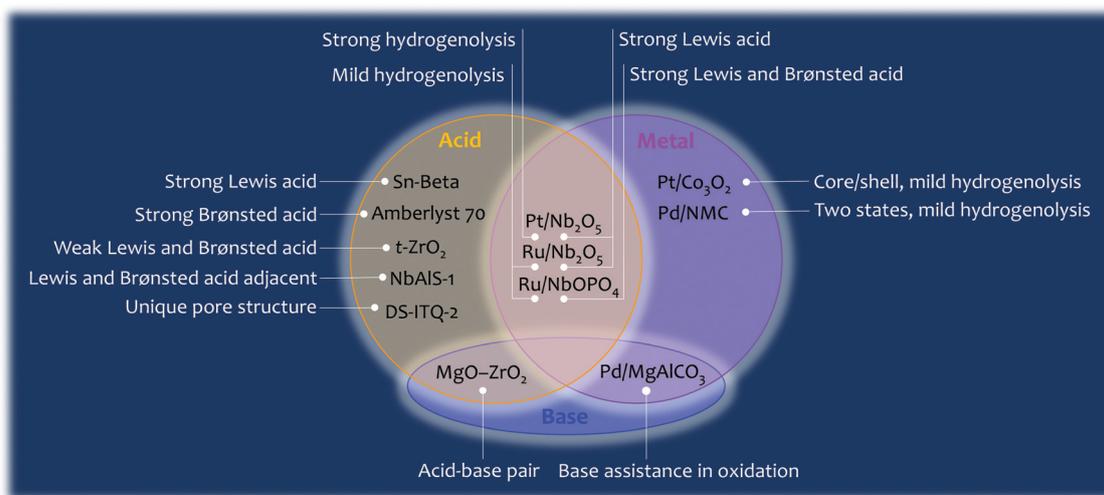
This journal is © The Royal Society of Chemistry 2021

Chem. Soc. Rev., 2021, 50, 11270–11292 | 11287

Fig. 13 An overview of the activity of selected heterogeneous catalysts discussed in this review.

protonated by the Brønsted acid, the $C_{aromatic}$–C bond is cleaved by β-scission. The –CHO and –OH groups can be activated by a strong Lewis acid (*e.g.*, Sn-beta), and the cleavage of the C–C bond of fructose undergoes retro-aldol condensation on Lewis acid sites. In terms of the cleavage of intramolecular C–O/C–C bonds (such as in GVL), the precise locations of the Brønsted and Lewis acid sites (NbAlS-1) and their close cooperation play a key role. The formation of C–O and C–C bonds is only involved in a few reactions for biomass conversion, such as the oxidation of –OH to –COOH, Diels–Alder cycloaddition to produce *p*-xylene, and aldol condensation for increasing the length of the carbon chain. In summary, the cleavage of C–O and C–C bonds is catalysed by acid sites and metal sites, while the formation of C–O and C–C bonds usually requires the participation of a base. Overall, reactions involving C–O or C–C bonds vary in different systems, and detailed studies of the reaction mechanism are required for the design of optimal catalysts for a given system.

6. Summary and outlook

The conversion of lignocellulosic biomass to useful carbon feedstocks is of great importance for the development of a sustainable and carbon-neutral economy. A number of research efforts have been devoted to developing efficient catalysts and catalytic systems for the conversion of lignin, cellulose and hemicellulose to value-added chemicals and liquid fuels. Lignin consists of aromatic units, linked by C–O and C–C bonds. To produce aromatics, the key step is to cleave C–O and C–C bonds selectively and to preserve aromatic functionalities in the meantime. Emerging niobium-based porous solids incorporating both NbO_x and Brønsted acid sites can catalyse the scission of both C–O and C–C bonds under an H_2 atmosphere, while largely preserving the aromatic functionalities with an arene selectivity up to ~70%. These promising systems give key insights into the design of new catalysts: (i) construction of cooperative catalytic sites (*e.g.*, early transition metals and strong Brønsted acid sites)

to promote the cleavage of C–O and C–C bonds; (ii) weakening the adsorption of benzene rings on the catalyst supports to hinder their hydrogenation; and (iii) optimising the active sites to promote the dissociation of hydrogen such as by using bimetallic nanoparticles.

The conversion of cellulose and hemicellulose to useful chemicals often involves cascade reactions. Dehydration and decarboxylation often occur on Brønsted acid sites. Isomerisation, retro-aldol condensation, hydride shift, and ring-opening prefer Lewis acid sites. Aldol condensation can be catalysed by either an acid or base. Subtle changes in the strength of the acid/base can greatly affect the performance of various catalysts. Hydrogenation, hydrogenolysis, hydrodeoxygenation and oxidation often need active metal sites, and the key to catalyst design is to precisely control the activity of these sites and to tune the microenvironments around these active sites, which all requires fundamental understanding of the reaction mechanism. It is therefore of critical importance to link catalyst design and catalysis testing to state-of-the-art structural and dynamic characterisation of the catalytic chemistries that underpin the product selectivity. Fundamental understanding of how catalysts function (or not) at a molecular level will enable us to 'see' and thus precisely manipulate the microenvironment to deliver the desired catalytic performance. A number of *operando* and *in situ* characterisation techniques have been employed to gain deep understanding, such as high-resolution synchrotron X-ray powder diffraction, inelastic neutron scattering, X-ray absorption spectroscopy and NMR spectroscopy. Vibrational spectroscopy is one of the most important techniques to capture the reaction intermediates and de-convolute the reaction network. While INS is usually collected at temperatures below 50 K to minimise the Debye–Waller effect, IR/Raman spectra can be collected at reaction temperatures, although their interpretation is often challenging and subject to uncertainties. The development of new measurement facilities to enable the simultaneous measurements of INS and optical spectroscopies would significantly promote the studies of reaction mechanisms by allowing the

11288 | *Chem. Soc. Rev.*, 2021, **50**, 11270–11292

This journal is © The Royal Society of Chemistry 2021

unambiguous assignment of vibrational modes with the aid of computational methods. The reaction mechanism discussed in this review will provide insights into further design and optimisation of future targets and identification of industrial applications in bio-refineries.

Conflicts of interest

The authors declare no competing financial interests.

Acknowledgements

References

1 X. Zhang, K. Wilson and A. F. Lee, *Chem. Rev.*, 2016, **116**, 12328–12368.

2 D. Yang, Q. Zhu, X. Sun, C. Chen, W. Guo, G. Yang and B. Han, *Angew. Chem., Int. Ed.*, 2020, **59**, 2354–2359.

3 L. T. Mika, E. Cséfalvay and Á. Németh, *Chem. Rev.*, 2018, **118**, 505–613.

4 D. M. Alonso, S. G. Wettstein and J. A. Dumesic, *Chem. Soc. Rev.*, 2012, **41**, 8075–8098.

5 D. Mohan, C. U. Pittman and P. H. Steele, *Energy Fuels*, 2006, **20**, 848–889.

6 A. V. Bridgwater, *Biomass Bioenergy*, 2012, **38**, 68–94.

7 Q. Xia, Z. Chen, Y. Shao, X. Gong, H. Wang, X. Liu, S. F. Parker, X. Han, S. Yang and Y. Wang, *Nat. Commun.*, 2016, **7**, 11162.

8 Q. Mei, H. Liu, X. Shen, Q. Meng, H. Liu, J. Xiang and B. Han, *Angew. Chem., Int. Ed.*, 2017, **56**, 14868–14872.

9 A. R. C. Morais, A. M. da Costa Lopes and R. Bogel-Łukasik, *Chem. Rev.*, 2015, **115**, 3–27.

10 Z. Zhang, J. Song and B. Han, *Chem. Rev.*, 2017, **117**, 6834–6880.

11 A. Brandt, J. Gräsvik, J. P. Hallett and T. Welton, *Green Chem.*, 2013, **15**, 550–583.

12 S. Xia, G. A. Baker, H. Li, S. Ravula and H. Zhao, *RSC Adv.*, 2014, **4**, 10586–10596.

13 A. Corma, S. Iborra and A. Velty, *Chem. Rev.*, 2007, **107**, 2411–2502.

14 J. Zakzeski, P. C. A. Bruijnincx, A. L. Jongerius and B. M. Weckhuysen, *Chem. Rev.*, 2010, **110**, 3552–3599.

15 M. Besson, P. Gallezot and C. Pinel, *Chem. Rev.*, 2014, **114**, 1827–1870.

16 C. Li, X. Zhao, A. Wang, G. W. Huber and T. Zhang, *Chem. Rev.*, 2015, **115**, 11559–11624.

17 W. Schutyser, T. Renders, S. V. den Bosch, S.-F. Koelewijn, G. T. Beckham and B. F. Sels, *Chem. Soc. Rev.*, 2018, **47**, 852–908.

18 D. Esposito and M. Antonietti, *Chem. Soc. Rev.*, 2015, **44**, 5821–5835.

19 P. Sudarsanam, R. Zhong, S. V. den Bosch, S. M. Coman, V. I. Parvulescu and B. F. Sels, *Chem. Soc. Rev.*, 2018, **47**, 8349–8402.

20 T. W. Walker, A. H. Motagamwala, J. A. Dumesic and G. W. Huber, *J. Catal.*, 2019, **369**, 518–525.

21 D. S. Sholl and R. P. Lively, *Nature*, 2016, **532**, 435–437.

22 G. W. Huber, S. Iborra and A. Corma, *Chem. Rev.*, 2006, **106**, 4044–4098.

23 P. Gallezot, *Chem. Soc. Rev.*, 2012, **41**, 1538–1558.

24 J. C. Serrano-Ruiz, R. Luque and A. Sepúlveda-Escribano, *Chem. Soc. Rev.*, 2011, **40**, 5266–5281.

25 C.-H. Zhou, X. Xia, C.-X. Lin, D.-S. Tong and J. Beltramini, *Chem. Soc. Rev.*, 2011, **40**, 5588–5617.

26 J. Iglesias, I. Martínez-Salazar, P. Maireles-Torres, D. M. Alonso, R. Mariscal and M. L. Granados, *Chem. Soc. Rev.*, 2020, **49**, 5704–5771.

27 H. Li, A. Bunrit, N. Li and F. Wang, *Chem. Soc. Rev.*, 2020, **49**, 3748–3763.

28 C. Mondelli, G. Gözaydın, N. Yan and J. Pérez-Ramírez, *Chem. Soc. Rev.*, 2020, **49**, 3764–3782.

29 G. R. Akien, L. Qi and I. T. Horváth, *Chem. Commun.*, 2012, **48**, 5850–5852.

30 T. Blasco, *Chem. Soc. Rev.*, 2010, **39**, 4685.

31 B. T. W. Lo, L. Ye and S. C. E. Tsang, *Chem*, 2018, **4**, 1778–1808.

32 M. A. Newton and W. van Beek, *Chem. Soc. Rev.*, 2010, **39**, 4845.

33 V. Van Speybroeck, K. Hemelsoet, L. Joos, M. Waroquier, R. G. Bell and C. R. A. Catlow, *Chem. Soc. Rev.*, 2015, **44**, 7044–7111.

34 Y. Shao, Q. Xia, L. Dong, X. Liu, X. Han, S. F. Parker, Y. Cheng, L. L. Daemen, A. J. Ramirez-Cuesta, S. Yang and Y. Wang, *Nat. Commun.*, 2017, **8**, 16104.

35 L. Dong, L. Lin, X. Han, X. Si, X. Liu, Y. Guo, F. Lu, S. Rudić, S. F. Parker, S. Yang and Y. Wang, *Chem*, 2019, **5**, 1521–1536.

36 L. Lin, A. M. Sheveleva, I. da Silva, C. M. A. Parlett, Z. Tang, Y. Liu, M. Fan, X. Han, J. H. Carter, F. Tuna, E. J. L. McInnes, Y. Cheng, L. L. Daemen, S. Rudić, A. J. Ramirez-Cuesta, C. C. Tang and S. Yang, *Nat. Mater.*, 2020, **19**, 86–93.

37 A. J. O'Malley, S. F. Parker and C. R. A. Catlow, *Chem. Commun.*, 2017, **53**, 12164–12176.

38 D. Lennon and S. F. Parker, *Acc. Chem. Res.*, 2014, **47**, 1220–1227.

39 P. W. Albers and S. F. Parker, *Adv. Catal.*, 2007, **51**, 99–132.

40 X. Han, H. G. W. Godfrey, L. Briggs, A. J. Davies, Y. Cheng, L. L. Daemen, A. M. Sheveleva, F. Tuna, E. J. L. McInnes, J. Sun, C. Drathen, M. W. George, A. J. Ramirez-Cuesta, K. M. Thomas, S. Yang and M. Schröder, *Nat. Mater.*, 2018, **17**, 691–696.

41 S. Yang, J. Sun, A. J. Ramirez-Cuesta, S. K. Callear, W. I. F. David, D. P. Anderson, R. Newby, A. J. Blake, J. E. Parker, C. C. Tang and M. Schröder, *Nat. Chem.*, 2012, **4**, 887–894.

42 S. Yang, A. J. Ramirez-Cuesta, R. Newby, V. Garcia-Sakai, P. Manuel, S. K. Callear, S. I. Campbell, C. C. Tang and M. Schröder, *Nat. Chem.*, 2015, **7**, 121–129.

43 L. Lin, Q. Mei, X. Han, S. F. Parker and S. Yang, *Top. Catal.*, 2021, **64**, 593–602.

44 M. Bender, *ChemBioEng Rev.*, 2014, **1**, 136–147.

45 M. Garside, *Global capacity of benzene 2017 & 2022*, Statista Inc., New York, 2020.

46 M. Garside, *Global production capacity of toluene 2018 & 2023*, Statista Inc., New York, 2019.

47 M. Garside, *Global xylene capacity projection 2019-2021*, Statista Inc., New York, p. 2021.

48 X. Shen, Q. Meng, Q. Mei, H. Liu, J. Yan, J. Song, D. Tan, B. Chen, Z. Zhang, G. Yang and B. Han, *Chem. Sci.*, 2020, **11**, 1347–1352.

49 Z. Ma, E. Troussard and J. A. van Bokhoven, *Appl. Catal., A*, 2012, **423–424**, 130–136.

50 O. Jan, R. Marchand, L. C. A. Anjos, G. V. S. Seufitelli, E. Nikolla and F. L. P. Resende, *Energy Fuels*, 2015, **29**, 1793–1800.

51 C. L. Williams, C.-C. Chang, P. Do, N. Nikbin, S. Caratzoulas, D. G. Vlachos, R. F. Lobo, W. Fan and P. J. Dauenhauer, *ACS Catal.*, 2012, **2**, 935–939.

52 L. Tao, T.-H. Yan, W. Li, Y. Zhao, Q. Zhang, Y.-M. Liu, M. M. Wright, Z.-H. Li, H.-Y. He and Y. Cao, *Chem*, 2018, **4**, 2212–2227.

53 V. J. Margarit, E. M. Gallego, C. Paris, M. Boronat, M. Moliner and A. Corma, *Green Chem.*, 2020, **22**, 5123–5131.

54 V. J. Margarit, M. E. Martínez-Armero, M. T. Navarro, C. Martínez and A. Corma, *Angew. Chem., Int. Ed.*, 2015, **54**, 13724–13728.

55 E. A. Uslamin, N. Kosinov, G. A. Filonenko, B. Mezari, E. Pidko and E. J. M. Hensen, *ACS Catal.*, 2019, **9**, 8547–8554.

56 F. Wang, X. Chu, P. Zhao, F. Zhu, Q. Li, F. Wu and G. Xiao, *Fuel*, 2020, **262**, 116538.

57 I. F. Teixeira, B. T. W. Lo, P. Kostetskyy, M. Stamatakis, L. Ye, C. C. Tang, G. Mpourmpakis and S. C. E. Tsang, *Angew. Chem., Int. Ed.*, 2016, **55**, 13061–13066.

58 P. S. Rezaei, H. Shafaghat and W. M. A. W. Daud, *Appl. Catal., A*, 2014, **469**, 490–511.

59 D. M. Alonso, S. G. Wettstein and J. A. Dumesic, *Green Chem.*, 2013, **15**, 584.

60 J. Q. Bond, D. M. Alonso, D. Wang, R. M. West and J. A. Dumesic, *Science*, 2010, **327**, 1110–1114.

61 J. J. Bozell, *Science*, 2010, **329**, 522–523.

62 D. Wang, S. H. Hakim, D. M. Alonso and J. A. Dumesic, *Chem. Commun.*, 2013, **49**, 7040–7042.

63 L. Ye, Q. Song, B. T. W. Lo, J. Zheng, D. Kong, C. A. Murray, C. C. Tang and S. C. E. Tsang, *Angew. Chem., Int. Ed.*, 2017, **56**, 10711–10716.

64 W. Lin, L. Ye, S. Wu, B. Lo, Y.-K. Peng, P. Zhao, I. McPherson and S. C. E. Tsang, *ChemSusChem*, 2018, **11**, 4214–4218.

65 J. C. Serrano-Ruiz, D. J. Braden, R. M. West and J. A. Dumesic, *Appl. Catal., B*, 2010, **100**, 184–189.

66 B. Donoeva and K. P. de Jong, *Nat. Mater.*, 2020, **19**, 5–6.

67 J. Q. Bond, C. S. Jungong and A. Chatzidimitriou, *J. Catal.*, 2016, **344**, 640–656.

68 B. T. W. Lo, L. Ye, J. Qu, J. Sun, J. Zheng, D. Kong, C. A. Murray, C. C. Tang and S. C. E. Tsang, *Angew. Chem., Int. Ed.*, 2016, **55**, 5981–5984.

69 M. A. Hillmyer, *Science*, 2017, **358**, 868–870.

70 J. M. Garcia and M. L. Robertson, *Science*, 2017, **358**, 870–872.

71 A.-C. Albertsson and M. Hakkarainen, *Science*, 2017, **358**, 872–873.

72 M. S. Holm, S. Saravanamurugan and E. Taarning, *Science*, 2010, **328**, 602–605.

73 R. F. Service, *Science*, 2006, **312**, 1861.

74 M. Dusselier, P. V. Wouwe, A. Dewaele, P. A. Jacobs and B. F. Sels, *Science*, 2015, **349**, 78–80.

75 T. Iwata, *Angew. Chem., Int. Ed.*, 2015, **54**, 3210–3215.

76 M. Xiong, D. K. Schneiderman, F. S. Bates, M. A. Hillmyer and K. Zhang, *Proc. Natl. Acad. Sci. U. S. A.*, 2014, **111**, 8357–8362.

77 A. Gandini, T. M. Lacerda, A. J. F. Carvalho and E. Trovatti, *Chem. Rev.*, 2016, **116**, 1637–1669.

78 M. Hong and E. Y.-X. Chen, *Nat. Chem.*, 2016, **8**, 42–49.

79 M. J. Sanford, L. Peña Carrodeguas, N. J. Van Zee, A. W. Kleij and G. W. Coates, *Macromolecules*, 2016, **49**, 6394–6400.

80 R. D. Clercq, M. Dusselier and B. F. Sels, *Green Chem.*, 2017, **19**, 5012–5040.

81 R. A. Gross and B. Kalra, *Science*, 2002, **297**, 803–807.

82 San Jose, *Global Lactic Acid Market*, PRWEB, California, 2012.

83 M. Dusselier, M. Mascal and B. F. Sels, in *Selective Catalysis for Renewable Feedstocks and Chemicals*, ed. K. M. Nicholas, Springer International Publishing, Cham, 2014, pp. 1–40.

84 Y. J. Wee, J. N. Kim and H. W. Ryu, *Food Technol. Biotechnol.*, 2006, **44**, 163–172.

85 W. Groot, J. van Krieken, O. Sliekersl and S. de Vos, *Poly(Lactic Acid)*, John Wiley & Sons, Ltd, 2010, pp. 1–18.

86 L. Li, F. Shen, R. L. Smith and X. Qi, *Green Chem.*, 2017, **19**, 76–81.

87 Y. Wang, W. Deng, B. Wang, Q. Zhang, X. Wan, Z. Tang, Y. Wang, C. Zhu, Z. Cao, G. Wang and H. Wan, *Nat. Commun.*, 2013, **4**, 2141.

88 F.-F. Wang, C.-L. Liu and W.-S. Dong, *Green Chem.*, 2013, **15**, 2091–2095.

89 W. Zeng, D. Cheng, F. Chen and X. Zhan, *Catal. Lett.*, 2009, **133**, 221.

90 F. Chambon, F. Rataboul, C. Pinel, A. Cabiac, E. Guillon and N. Essayem, *Appl. Catal., B*, 2011, **105**, 171–181.

91 Q. Guo, F. Fan, E. A. Pidko, W. N. P. van der Graaff, Z. Feng, C. Li and E. J. M. Hensen, *ChemSusChem*, 2013, **6**, 1352–1356.

92 K. Shimizu, H. Furukawa, N. Kobayashi, Y. Itaya and A. Satsuma, *Green Chem.*, 2009, **11**, 1627–1632.

93 C. C. Chang, H. Je Cho, Z. Wang, X. Wang and W. Fan, *Green Chem.*, 2015, **17**, 2943–2951.

11290 | *Chem. Soc. Rev.*, 2021, **50**, 11270–11292

This journal is © The Royal Society of Chemistry 2021

94 C. Luo, S. Wang and H. Liu, *Angew. Chem., Int. Ed.*, 2007, **46**, 7636–7639.

95 S. J. Dee and A. T. Bell, *ChemSusChem*, 2011, **4**, 1166–1173.

96 N. Shimada, H. Kawamoto and S. Saka, *Carbohydr. Res.*, 2007, **342**, 1373–1377.

97 Y. Román-Leshkov, M. Moliner, J. A. Labinger and M. E. Davis, *Angew. Chem., Int. Ed.*, 2010, **49**, 8954–8957.

98 M. Moliner, Y. Román-Leshkov and M. E. Davis, *Proc. Natl. Acad. Sci. U. S. A.*, 2010, **107**, 6164–6168.

99 R. Bermejo-Deval, R. S. Assary, E. Nikolla, M. Moliner, Y. Román-Leshkov, S.-J. Hwang, A. Palsdottir, D. Silverman, R. F. Lobo, L. A. Curtiss and M. E. Davis, *Proc. Natl. Acad. Sci. U. S. A.*, 2012, **109**, 9727–9732.

100 S. G. Elliot, E. Taarning, R. Madsen and S. Meier, *ChemCatChem*, 2018, **10**, 1414–1419.

101 X. Yang, B. Lv, T. Lu, Y. Su and L. Zhou, *Catal. Sci. Technol.*, 2020, **10**, 700–709.

102 S. Yamaguchi, M. Yabushita, M. Kim, J. Hirayama, K. Motokura, A. Fukuoka and K. Nakajima, *ACS Sustainable Chem. Eng.*, 2018, **6**, 8113–8117.

103 M. Kim, S. Ronchetti, B. Onida, N. Ichikuni, A. Fukuoka, H. Kato and K. Nakajima, *ChemCatChem*, 2020, **12**, 350–359.

104 Y. Sun, L. Shi, H. Wang, G. Miao, L. Kong, S. Li and Y. Sun, *Sustainable Energy Fuels*, 2019, **3**, 1163–1171.

105 M. Dusselier and B. F. Sels, in *Selective Catalysis for Renewable Feedstocks and Chemicals*, ed. K. M. Nicholas, Springer International Publishing, Cham, 2014, pp. 85–126.

106 E. Taarning, S. Saravanamurugan, M. Spangsberg Holm, J. Xiong, R. M. West and C. H. Christensen, *ChemSusChem*, 2009, **2**, 625–627.

107 K. Nakajima, J. Hirata, M. Kim, N. K. Gupta, T. Murayama, A. Yoshida, N. Hiyoshi, A. Fukuoka and W. Ueda, *ACS Catal.*, 2018, **8**, 283–290.

108 X. Wang, Y. Song, L. Huang, H. Wang, C. Huang and C. Li, *Catal. Sci. Technol.*, 2019, **9**, 1669–1679.

109 M. Xia, W. Dong, M. Gu, C. Chang, Z. Shen and Y. Zhang, *RSC Adv.*, 2018, **8**, 8965–8975.

110 X. Yang, J. Bian, J. Huang, W. Xin, T. Lu, C. Chen, Y. Su, L. Zhou, F. Wang and J. Xu, *Green Chem.*, 2017, **19**, 692–701.

111 X. Yang, Y. Liu, X. Li, J. Ren, L. Zhou, T. Lu and Y. Su, *ACS Sustainable Chem. Eng.*, 2018, **6**, 8256–8265.

112 S. Tolborg, I. Sádaba, C. M. Osmundsen, P. Fristrup, M. S. Holm and E. Taarning, *ChemSusChem*, 2015, **8**, 613–617.

113 F. de Clippel, M. Dusselier, R. Van Rompaey, P. Vanelderen, J. Dijkmans, E. Makshina, L. Giebeler, S. Oswald, G. V. Baron, J. F. M. Denayer, P. P. Pescarmona, P. A. Jacobs and B. F. Sels, *J. Am. Chem. Soc.*, 2012, **134**, 10089–10101.

114 M. Orazov and M. E. Davis, *Proc. Natl. Acad. Sci. U. S. A.*, 2015, **112**, 11777–11782.

115 L. Yang, X. Yang, E. Tian, V. Vattipalli, W. Fan and H. Lin, *J. Catal.*, 2016, **333**, 207–216.

116 L. Yang, X. Yang, E. Tian and H. Lin, *ChemSusChem*, 2016, **9**, 36–41.

117 D. Verma, R. Insyani, Y.-W. Suh, S. M. Kim, S. K. Kim and J. Kim, *Green Chem.*, 2017, **19**, 1969–1982.

118 F. F. Wang, J. Liu, H. Li, C.-L. Liu, R. Z. Yang and W. S. Dong, *Green Chem.*, 2015, **17**, 2455–2463.

119 A. A. Marianou, C. C. Michailof, D. Ipsakis, K. Triantafyllidis and A. A. Lappas, *Green Chem.*, 2019, **21**, 6161–6178.

120 A. H. Motagamwala, W. Won, C. Sener, D. M. Alonso, C. T. Maravelias and J. A. Dumesic, *Sci. Adv.*, 2018, **4**, eaap9722.

121 M. Sajid, X. Zhao and D. Liu, *Green Chem.*, 2018, **20**, 5427–5453.

122 Y. Wang, K. Yu, D. Lei, W. Si, Y. Feng, L.-L. Lou and S. Liu, *ACS Sustainable Chem. Eng.*, 2016, **4**, 4752–4761.

123 C. O. Tuck, E. Pérez, I. T. Horváth, R. A. Sheldon and M. Poliakoff, *Science*, 2012, **337**, 695–699.

124 G. W. Huber, J. N. Chheda, C. J. Barrett and J. A. Dumesic, *Science*, 2005, **308**, 1446–1450.

125 T. D. Matson, K. Barta, A. V. Iretskii and P. C. Ford, *J. Am. Chem. Soc.*, 2011, **133**, 14090–14097.

126 Y. Román-Leshkov, C. J. Barrett, Z. Y. Liu and J. A. Dumesic, *Nature*, 2007, **447**, 982–985.

127 E. L. Kunkes, D. A. Simonetti, R. M. West, J. C. Serrano-Ruiz, C. A. Gärtner and J. A. Dumesic, *Science*, 2008, **322**, 417–421.

128 X. Han, Y. Guo, X. Liu, Q. Xia and Y. Wang, *Catal. Today*, 2019, **319**, 2–13.

129 C. Wang, X. Zhang, Q. Liu, Q. Zhang, L. Chen and L. Ma, *Fuel Process. Technol.*, 2020, **208**, 106485.

130 Y. Nakagawa, M. Tamura and K. Tomishige, *Fuel Process. Technol.*, 2019, **193**, 404–422.

131 C. Moreau, R. Durand, S. Razigade, J. Duhamet, P. Faugeras, P. Rivalier, P. Ros and G. Avignon, *Appl. Catal., A*, 1996, **145**, 211–224.

132 T. Chhabra, A. Bahuguna, S. S. Dhankhar, C. M. Nagaraja and V. Krishnan, *Green Chem.*, 2019, **21**, 6012–6026.

133 G. Yang, E. A. Pidko and E. J. M. Hensen, *J. Catal.*, 2012, **295**, 122–132.

134 J. Zhang, A. Das, R. S. Assary, L. A. Curtiss and E. Weitz, *Appl. Catal., B*, 2016, **181**, 874–887.

135 Y. Román-Leshkov, J. N. Chheda and J. A. Dumesic, *Science*, 2006, **312**, 1933–1937.

136 Q. Sun, S. Wang, B. Aguila, X. Meng, S. Ma and F. S. Xiao, *Nat. Commun.*, 2018, **9**, 3236.

137 J. Luo, H. Yun, A. V. Mironenko, K. Goulas, J. D. Lee, M. Monai, C. Wang, V. Vorotnikov, C. B. Murray, D. G. Vlachos, P. Fornasiero and R. J. Gorte, *ACS Catal.*, 2016, **6**, 4095–4104.

138 R. Gunawan, H. S. Cahyadi, R. Insyani, S. K. Kwak and J. Kim, *J. Phys. Chem. C*, 2021, **125**, 10295–10317.

139 S. Chen, R. Wojcieszak, F. Dumeignil, E. Marceau and S. Royer, *Chem. Rev.*, 2018, **118**, 11023–11117.

140 J. Luo, J. D. Lee, H. Yun, C. Wang, M. Monai, C. B. Murray, P. Fornasiero and R. J. Gorte, *Appl. Catal., B*, 2016, **199**, 439–446.

141 G. H. Wang, J. Hilgert, F. H. Richter, F. Wang, H. J. Bongard, B. Spliethoff, C. Weidenthaler and F. Schüth, *Nat. Mater.*, 2014, **13**, 293–300.

This journal is © The Royal Society of Chemistry 2021

Chem. Soc. Rev., 2021, **50**, 11270–11292 | 11291

142 B. Chen, F. Li, Z. Huang and G. Yuan, *Appl. Catal., B*, 2017, **200**, 192–199.

143 C. Zhu, H. Wang, H. Li, B. Cai, W. Lv, C. Cai, C. Wang, L. Yan, Q. Liu and L. Ma, *ACS Sustainable Chem. Eng.*, 2019, **7**, 19556–19569.

144 G. Meng, K. Ji, W. Zhang, Y. Kang, Y. Wang, P. Zhang, Y. G. Wang, J. Li, T. Cui, X. Sun, T. Tan, D. Wang and Y. Li, *Chem. Sci.*, 2021, **12**, 4139–4146.

145 B. Hu, L. Warczinski, X. Li, M. Lu, J. Bitzer, M. Heidelmann, T. Eckhard, Q. Fu, J. Schulwitz, M. Merko, M. Li, W. Kleist, C. Hättig, M. Muhler and B. Peng, *Angew. Chem., Int. Ed.*, 2021, **60**, 6807–6815.

146 J. Zhao, M. Liu, G. Fan, L. Yang and F. Li, *Ind. Eng. Chem. Res.*, 2021, **60**, 5826–5837.

147 Y. Sun, C. Xiong, Q. Liu, J. Zhang, X. Tang, X. Zeng, S. Liu and L. Lin, *Ind. Eng. Chem. Res.*, 2019, **58**, 5414–5422.

148 T. Thananatthanachon and T. B. Rauchfuss, *Angew. Chem., Int. Ed.*, 2010, **49**, 6616–6618.

149 H. Wang, C. Zhu, D. Li, Q. Liu, J. Tan, C. Wang, C. Cai and L. Ma, *Renewable Sustainable Energy Rev.*, 2019, **103**, 227–247.

150 J. Li, Z. Song, Y. Hou, Z. Li, C. Xu, C.-L. Liu and W.-S. Dong, *ACS Appl. Mater. Interfaces*, 2019, **11**, 12481–12491.

151 R. Insyani, D. Verma, H. S. Cahyadi, S. M. Kim, S. K. Kim, N. Karanwal and J. Kim, *Appl. Catal., B*, 2019, **243**, 337–354.

152 L. Jin, W. Li, Q. Liu, L. Ma, C. Hu, A. T. Ogunbiyi, M. Wu and Q. Zhang, *Bioresour. Technol.*, 2020, **297**, 122492.

153 L. Jin, W. Li, Q. Liu, L. Ma, S. Li, Y. Liu, B. Zhang and Q. Zhang, *Fuel Process. Technol.*, 2019, **196**, 106161.

154 A. Romero, A. Nieto-Márquez, N. Essayem, E. Alonso and C. Pinel, *Microporous Mesoporous Mater.*, 2019, **286**, 25–35.

155 G. W. Huber, R. D. Cortright and J. A. Dumesic, *Angew. Chem., Int. Ed.*, 2004, **43**, 1549–1551.

156 S. Liu, M. Tamura, Y. Nakagawa and K. Tomishige, *ACS Sustainable Chem. Eng.*, 2014, **2**, 1819–1827.

157 L. Faba, E. Díaz and S. Ordóñez, *Appl. Catal., B*, 2012, **113–114**, 201–211.

11292 | *Chem. Soc. Rev.*, 2021, **50**, 11270–11292

This journal is © The Royal Society of Chemistry 2021